

1 **History of carbonate ion concentration over the last 100 million**  
2 **years II: Revised calculations and new data**

3 Richard E. Zeebe<sup>1,\*</sup> and Toby Tyrrell<sup>2</sup>

4 \*Corresponding Author.

5 <sup>1</sup>School of Ocean and Earth Science and Technology, University of Hawaii at Manoa, 1000 Pope Road, MSB 629, Honolulu, HI  
6 96822, USA. zeebe@hawaii.edu

7 <sup>2</sup>Ocean and Earth Science, University of Southampton, European Way, Southampton SO14 3ZH, UK. Toby.Tyrrell@soton.ac.uk

8 Revised ms V2.9

9 February 2, 2019

10 Resubmitted to *Geochim. Cosmochim. Acta*

11

12

**Abstract.** In an earlier contribution to this journal, we provided a reconstruction of seawater carbonate ion concentration over the last 100 million years (Tyrrell, T. and Zeebe, R.E., *Geochim. Cosmoch. Acta*, 68, 3521-3530, 2004; TZo4 hereafter). Since then, multiple new and more robust data sets on past ocean carbonate chemistry, atmospheric CO<sub>2</sub>, and major ion seawater composition have emerged, which prompt new CO<sub>2</sub> system reconstructions. In addition, we have gained new insight into the effects of past major ion seawater composition on equilibrium constants affecting CO<sub>2</sub> system calculations — most notably due to sulfate. Here we present new reconstructions of past ocean carbonate chemistry and atmospheric CO<sub>2</sub> based on new data and revised calculations, including error analysis. We also provide simple corrections for past equilibrium constants, supported by experimental data and well-suited for numerical models and observational studies on multi-million year time scales. Our updated result for just the seawater carbonate ion concentration (~2.3 to 4-fold lower 100 Myr ago) is similar to TZo4, indicating that our core approach is robust. However, all revised reconstructions using new alkenone and boron data now suggest that long-term ocean inventories of total dissolved inorganic carbon (DIC) and total alkalinity (TA) were similar to modern over the Cenozoic. This result contrasts strongly with one of TZo4's scenarios, which featured high Paleocene-Eocene DIC/TA inventories and was based on boron-derived *p*H values that have recently been revised. Because the carbonate system has two degrees of freedom, consistency checks can be made when three or more parameters are determined. Overall, our estimated long-term trends in CO<sub>2</sub> system parameters across the Cenozoic appear consistent, regardless of whether we combine our carbonate ion concentration with alkenone-derived *p*CO<sub>2</sub> or boron-derived *p*H. Our results suggest convergence towards a consistent picture of Cenozoic atmospheric CO<sub>2</sub> and seawater chemistry. Finally, we identify changes in past seawater sulfate as a conceptual and practical problem for seawater *p*H reconstructions.

## 39 **1 Introduction**

40 Reconstructing past atmospheric CO<sub>2</sub> concentrations and ocean carbonate  
 41 chemistry is critical for understanding carbon cycle-climate feedbacks, climate  
 42 sensitivity, ocean acidification and more (for recent reviews, see [Kump et al., 2009](#);  
 43 [Hönisch et al., 2012](#); [Zeebe, 2012a](#); [Rohling et al., 2012](#)). [Tyrrell and Zeebe \(2004\)](#)  
 44 (TZo<sub>4</sub>) reconstructed the ocean’s carbonate ion concentration ([CO<sub>3</sub><sup>2-</sup>]) based on a  
 45 simple but effective idea using the CaCO<sub>3</sub> saturation state ( $\Omega$ ) of seawater:

$$\Omega = \frac{[\text{Ca}^{2+}] [\text{CO}_3^{2-}]}{K_{\text{sp}}^*}, \quad (1)$$

46 where [Ca<sup>2+</sup>] is the dissolved calcium concentration and  $K_{\text{sp}}^*$  is the solubility product of  
 47 calcite or aragonite; square brackets denote stoichiometric concentrations. Briefly, given  
 48 information on past [Ca<sup>2+</sup>],  $K_{\text{sp}}^*$ , and  $\Omega$ , Eq. (1) can be solved for [CO<sub>3</sub><sup>2-</sup>] — an approach  
 49 that has been widely cited and applied since (e.g., [Locklair and Lerman, 2005](#); [Pearson](#)  
 50 [et al., 2009](#); [Seki et al., 2010](#); [Bartoli et al., 2011](#); [Gillis and Coogan, 2011](#); [Raven and](#)  
 51 [Crawfurd, 2012](#); [Boudreau and Luo, 2017](#); [Sosdian et al., 2018](#)). Prior to TZo<sub>4</sub>, attempts  
 52 to reconstruct surface ocean carbonate chemistry considered calcite saturation as well  
 53 but usually assumed constant seawater [Ca<sup>2+</sup>] in the past (e.g. [Sundquist, 1986](#); [Caldeira](#)  
 54 [and Berner, 1999](#); [Sundquist, 1999](#)). TZo<sub>4</sub> also pointed out that corrections for past  
 55 equilibrium constants due to changes in major ion seawater composition are warranted,  
 56 which has subsequently been considered in other applications, including numerical  
 57 models (e.g., [Zeebe et al., 2009](#); [Ridgwell and Schmidt, 2010](#); [Zeebe, 2012b](#)).

58 Combining [CO<sub>3</sub><sup>2-</sup>] with a second carbonate chemistry parameter allows full CO<sub>2</sub>  
 59 system reconstructions as two parameters are required to determine the system (plus  
 60 temperature and salinity estimates) (e.g., [Zeebe and Wolf-Gladrow, 2001](#)). As the second  
 61 parameter, TZo<sub>4</sub> used GEOCARB  $p\text{CO}_2$  ([Berner and Kothavala, 2001](#)) and a single  
 62  $\delta^{11}\text{B}$ -based  $p\text{H}$  record available at the time ([Pearson and Palmer, 2000](#)), the latter of  
 63 which has recently been revised ([Anagnostou et al., 2016](#)). Since then, multiple new and

64 more robust data sets on past ocean carbonate chemistry, atmospheric CO<sub>2</sub>, and major  
65 ion seawater composition have been published. This has prompted us to perform new  
66 CO<sub>2</sub> system reconstructions over the last 100 Myr, including error analysis. We also  
67 provide simple, updated corrections for past equilibrium constants that are supported by  
68 experimental data and can easily be used in numerical models and observational studies  
69 on multi-million year time scales.

## 70 **2 Past Major Ion Seawater Composition**

71 As in TZ04, we use fluid inclusion data in this study to estimate past changes in  
72 major ion composition (Fig. 1a) (Horita et al., 2002; Lowenstein et al., 2003; Timofeeff  
73 et al., 2006; Brennan et al., 2013). While such estimates come with uncertainties (see  
74 original references for details), the general trends are consistent with other independent  
75 evidence for the seawater Mg/Ca ratio (Fig. 1b) such as the chemical compositions of  
76 calcifier fossils, inorganic calcite veins, etc. (see e.g., Stanley and Hardie, 1998; Dickson,  
77 2002; Montañez, 2002; Tyrrell and Zeebe, 2004; Coggon et al., 2010; Evans and Müller,  
78 2012; Rausch et al., 2013; Gothmann et al., 2015, and references therein). Our standard  
79 error envelopes (Fig. 1) assume zero errors at present (known modern values) and  
80 gradually increasing errors in the past. Note that given the long residence times of Ca<sup>2+</sup>  
81 and Mg<sup>2+</sup>, rapid swings that could be inferred from some of the data in Fig. 1a and b are  
82 implausible. For uncertainties in fluid inclusion reconstructions resulting from the value  
83 used for the product of [Ca<sup>2+</sup>] × [SO<sub>4</sub><sup>2-</sup>], see Section 5.3.2. Recent efforts to reconstruct  
84 seawater [Ca<sup>2+</sup>] based on foraminiferal Na/Ca ratios also yield trends broadly consistent  
85 with those from fluid inclusions (Hauzer et al., 2018; Zhou et al., 2018).

86 Past major ion changes (Fig. 1) have important implications for our reconstructions.  
87 First, given Eq. (1), one key consequence of higher [Ca<sup>2+</sup>] in the past (Fig. 1) is that [CO<sub>3</sub><sup>2-</sup>]  
88 must have been lower (everything else being equal). It turns out that this overriding

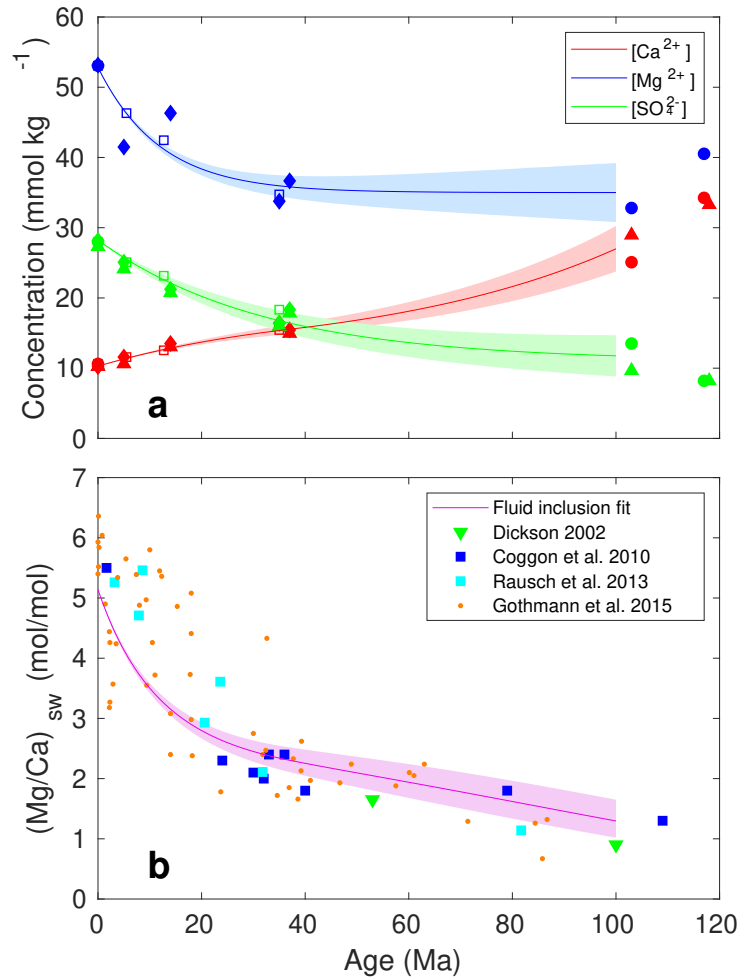


**Figure 1:** (a) Past changes in  $[\text{Ca}^{2+}]$ ,  $[\text{Mg}^{2+}]$ , and  $[\text{SO}_4^{2-}]$  based on fluid inclusion data. Diamonds: Horita et al. (2002), triangles: Lowenstein et al. (2003), circles: Timofeeff et al. (2006), squares: Brennan et al. (2013). These studies assumed constant, modern  $[\text{Ca}^{2+}] \times [\text{SO}_4^{2-}]$  over time to derive  $[\text{Ca}^{2+}]$  and  $[\text{SO}_4^{2-}]$  as shown, to which our estimated standard error envelopes apply (shaded areas). For errors from different  $[\text{Ca}^{2+}] \times [\text{SO}_4^{2-}]$  values, see Section 5.3.2. Concentrations were converted from  $\text{mmol kg}^{-1}\text{-H}_2\text{O}$  to  $\text{mmol kg}^{-1}\text{-solution}$  using  $S = 35$ . Solid lines are exponential fits (standard fits hereafter) to obtain differentiable (smooth) curves over 100 Myr (see text). (b) Independent estimates of past seawater Mg/Ca ratios from echinoderms (Dickson, 2002),  $\text{CaCO}_3$  veins (Coggon et al., 2010; Rausch et al., 2013), and fossil corals (Gothmann et al., 2015). The purple line and envelope show seawater Mg/Ca and propagated errors from fit to fluid inclusions in (a). Standard envelopes assume zero errors at present (known modern values) and gradually increasing errors in the past. Given the long residence times of  $\text{Ca}^{2+}$  and  $\text{Mg}^{2+}$ , rapid swings that might be inferred from some of the data in (a) and (b) are implausible.

89 consideration dominates despite past changes in  $\Omega$  and  $K_{\text{sp}}^*$  (see Sections 4 and 5). The  
 90 two- to three-fold decline in  $[\text{Ca}^{2+}]$  over the past 100 Ma forced a compensating large  
 91 increase in  $[\text{CO}_3^{2-}]$ . Second, chemical equilibrium constants ( $K^*$ 's) used to calculate

ocean carbonate chemistry depend on the major constituents of seawater, which have varied in the past. Hence  $K^*$ 's require corrections over time, which we provide below (see Section 3).

Exponential functions were fit over 100 Myr to the estimated concentrations from fluid inclusions for  $[\text{Ca}^{2+}]$ ,  $[\text{Mg}^{2+}]$ , and  $[\text{SO}_4^{2-}]$ ;  $x_j$ 's for short, where  $j = 1, 2, 3$  (see Fig. 1a, Table 1):

$$x(t) = (x' - x'') e^{-(t-t_1)/\tau} + x'' , \quad (2)$$

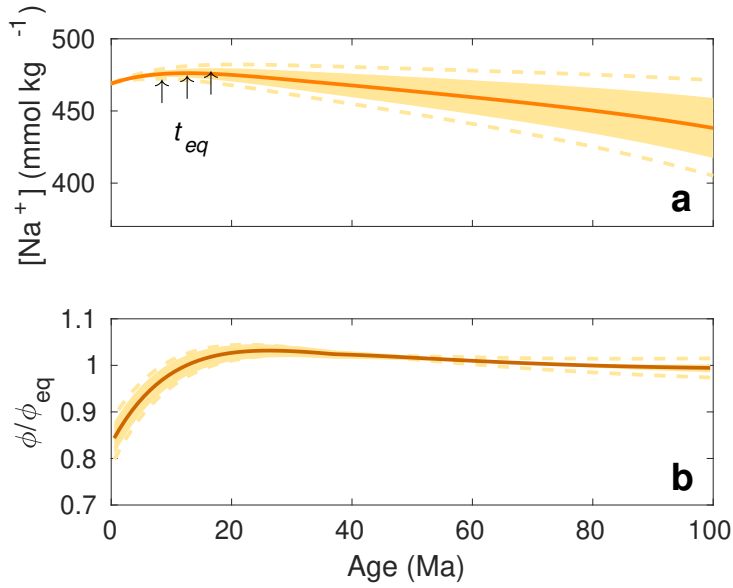
where  $x'$ ,  $x''$ ,  $t_1$ , and  $\tau$  are constants (see Table 1). Note that there is no mechanistic reason for an exponential fit. In fact, between 37 and 100 Ma, the fit is unconstrained and one could select a linear fit as the parsimonious model. We only use exponentials here to obtain differentiable (smooth) curves over 100 Myr. Below, we will discuss flux estimates based on derivatives, which would produce artificial flux spikes for non-smooth curves.

Table 1.: Fit parameters for Eq. (2).

		$x'$	$x''$	$t_1$	$\tau$
$\text{Ca}^{2+}$	<sup>a</sup>	10.280	19.000	0	40.000
$\text{Ca}^{2+}$	<sup>b</sup>	15.542	11.478	37	-47.011
$\text{Mg}^{2+}$	<sup>c</sup>	52.820	35.000	0	12.000
$\text{SO}_4^{2-}$	<sup>c</sup>	28.240	11.000	0	32.000

<sup>a</sup> $t = [0 \ 37]$ ; <sup>b</sup> $t = [37 \ 100]$ ; <sup>c</sup> $t = [0 \ 100]$  Ma.

One critical requirement for past reconstructions of seawater chemistry is that charge balance must be maintained. That is, the sum of all positive charges must equal the sum of all negative charges at all times. It turns out that the estimated changes in  $x_j$ 's alone (standard fits, Fig. 1a) would produce a charge imbalance of up to +30 mmol kg<sup>-1</sup> in the past (the  $[\text{SO}_4^{2-}]$  decline remains essentially unbalanced), although the magnitude of the imbalance depends on the product of  $[\text{Ca}^{2+}] \times [\text{SO}_4^{2-}]$  assumed in the fluid inclusion



**Figure 2.:** (a) Past seawater  $[\text{Na}^+]$  derived from fits to fluid inclusion data (Fig. 1a) and charge balance (see text). The envelope represents standard errors propagated from Fig. 1a. Dashed lines estimate errors due to different  $[\text{Ca}^{2+}] \times [\text{SO}_4^{2-}]$  values by doubling the standard errors for  $[\text{Ca}^{2+}]$  and  $[\text{SO}_4^{2-}]$ , see Section 5.3.2. (b) Inferred  $\text{Na}^+$  influx based on Eq. (3). Note that the steady-state flux ( $\phi_{eq}$ ) corresponds to time  $t_{eq}$  where  $[\text{Na}^+]$  is at maximum ( $d[\text{Na}^+]/dt = 0$ ), not to  $t = 0$ . The ratio  $\phi/\phi_{eq} = 1$  occurs at  $t_{eq}$ , which varies for each scenario (arrows) and in turn give different flux estimates at  $t = 0$ .

110 studies, see Section 5.3.2. If correct, the imbalance is significant and was unlikely  
 111 compensated for by minor constituents. Rather, other major ions would have to make  
 112 up for the imbalance such as  $\text{Cl}^-$ ,  $\text{Na}^+$ , and  $\text{K}^+$ .  $\text{Cl}^-$  has a very long residence time and  
 113  $[\text{K}^+]$  probably changed very little over the Phanerozoic (Horita et al., 2002). This leaves  
 114 changes in  $[\text{Na}^+]$  to maintain charge balance. In fact, this assumption has been made to  
 115 reconstruct  $[\text{Na}^+]$  in the past (e.g., Timofeeff et al., 2006; Brennan et al., 2013). If the  
 116 same assumption is made here, it would lead to  $\sim 30 \text{ mmol kg}^{-1}$  lower  $[\text{Na}^+]$  at 100 Ma  
 117 for the standard scenario (Fig. 2). Do such changes in  $\text{Na}^+$  inventory and flux appear  
 118 feasible, given sodium's residence time in the ocean?

119 The change in  $\text{Na}^+$  influx ( $\phi$ ) required to produce the estimated past change in the  
 120 ocean's  $[\text{Na}^+]$  inventory (Fig. 2) may be estimated from:

$$\frac{dM_{\text{Na}^+}}{dt} = \phi - (1/\tau_{\text{Na}^+}) \cdot M_{\text{Na}^+}, \quad (3)$$

121 where  $M_{\text{Na}^+}$  is the  $\text{Na}^+$  inventory and  $\tau_{\text{Na}^+}$  is the residence time of  $\text{Na}^+$ . Given  $M_{\text{Na}^+}$  over  
 122 time (Fig. 2), its derivative can be calculated. Using  $\tau_{\text{Na}^+} \simeq 50$  Myr (Berner and Berner,  
 123 2012; Lécuyer, 2016), Eq. (3) can then be solved for  $\phi$ . As a result, the  $\text{Na}^+$  influx would  
 124 have to change by less than  $\sim 20\%$  over the past 100 Myr to explain the seawater  $\text{Na}^+$   
 125 concentrations as implied by fluid inclusions (Fig. 2). However, note that these estimates  
 126 have large uncertainties beyond those suggested by the error envelopes, including  
 127 intrinsic errors in individual fluid inclusion reconstructions (e.g., Section 5.3.2),  
 128 assumptions about constant  $[\text{Cl}^-]$  and  $[\text{K}^+]$ ,  $\text{Na}^+$  residence time, neglecting changes  
 129 in minor constituents, etc. Note also that it is not clear what would have caused the  
 130 relatively rapid decrease in  $\text{Na}^+$  flux over the past 10-15 Myr (Fig. 2). Finally, changes in  
 131  $[\text{Na}^+]$  of the indicated magnitude have a small effect on our overall results. For example,  
 132 calculated sensitivity parameters for past  $K^*$  corrections (see Section 3.2) show modest  
 133 changes with  $[\text{Na}^+]$  (Tables 2 and D1) and our carbonate chemistry reconstructions are  
 134 not overly sensitive to changes in  $K^*$ 's (see Section 5.3).

## 135 2.1 Artificial paleo-seawater

136 Regardless of uncertainties in past major ion changes, it may be desirable to  
 137 prepare artificial seawater with major ion composition different from modern, e.g., for  
 138 geochemical or biological purposes (e.g., Mucci and Morse, 1984; Ries, 2004; Haynes  
 139 et al., 2017; Zeebe and Tyrrell, 2018). If such artificial seawater were to resemble major  
 140 ion changes as discussed here, including  $[\text{Ca}^{2+}]$ ,  $[\text{Mg}^{2+}]$ , and  $[\text{SO}_4^{2-}]$ , one option is to  
 141 vary the salt concentrations of  $\text{NaCl}$ ,  $\text{CaCl}_2$ ,  $\text{MgCl}_2$ , and  $\text{Na}_2\text{SO}_4$ . However, note that  
 142 this is only one option and does not necessarily reflect actual paleo-seawater changes.

143 If the goal is, for instance, to maintain charge balance by adjusting  $[\text{Na}^+]$  at constant  
 144  $[\text{Cl}^-]$ , then mole-by-mole differences in salt additions/reductions ( $\Delta$ 's) may be obtained  
 145 from  $\Delta\text{NaCl} = n\Delta\text{MA}_2$ , where  $\text{M} = \text{Ca}$  or  $\text{Mg}$ ,  $\text{A} = \text{Cl}$ , and  $n = -2$ . That is, for example,  
 146 a rise in  $[\text{Ca}^{2+}]$  by  $x$  (in appropriate units) is compensated for by a  $2x$ -drop in  $[\text{Na}^+]$ .



147 Changes in  $[\text{SO}_4^{2-}]$  may be achieved by simply adjusting the amount of  $\text{Na}_2\text{SO}_4$  added.  
 148 If the goal is to maintain constant ionic strength ( $I$ ) by adjusting  $\text{NaCl}$ , then  $n = -3$  for  
 149 the above recipe; furthermore  $\Delta\text{NaCl} = n\Delta\text{Na}_2\text{SO}_4$ . The factor 3 arises from the fact  
 150 that the ions of the salt with one doubly charged ion (say  $\text{MA}_2$  or  $\text{Na}_2\text{SO}_4$ ) contribute  
 151 3 units to  $\Delta I = \sum z_i^2 x_i / 2 = (2^2 x + 1^2 \cdot 2x) / 2 = 3x$ , whereas  $\text{NaCl}$  contributes only one  
 152 unit:  $(1^2 x + 1^2 x) / 2 = 1x$ . For this constant ionic strength scenario, of course both total  
 153  $[\text{Na}^+]$  and  $[\text{Cl}^-]$  change, with their net change being given by the sum of the individual  
 154 additions/reductions of the salts that contain them. For example, raising  $[\text{SO}_4^{2-}]$  by  
 155  $x$  via  $\text{Na}_2\text{SO}_4$  addition requires  $\text{NaCl}$  reduction by  $3x$ , hence a net  $[\text{Na}^+]$  change by  
 156  $2x - 3x = -x$ . The charge balance and constant ionic strength scenarios appear relevant  
 157 to a variety of problems and have been applied in chemical and physiological studies.  
 158 Indeed, charge and ionic strength are likely critical for a variety of geochemical and  
 159 biological processes given their nature of ionic interactions, rather than, for instance,  
 160 total salt content (mass). We will therefore provide corrections for stoichiometric  
 161 equilibrium constants for the charge balance and constant ionic strength scenarios below  
 162 (Section 3.2, Appendix D).

### 163 **3 Effects of $[\text{Ca}^{2+}]$ , $[\text{Mg}^{2+}]$ , and $[\text{SO}_4^{2-}]$ on Stoichiometric** 164 **Equilibrium Constants**

165 As detailed in Section 2, there is compelling evidence for large changes in major  
 166 ion seawater composition over the last 100 Myr. Among the major ions, changes in  
 167  $[\text{Ca}^{2+}]$ ,  $[\text{Mg}^{2+}]$ , and  $[\text{SO}_4^{2-}]$  are most critical for our carbonate chemistry reconstructions  
 168 through their effect on  $[\text{CO}_3^{2-}]$  (for  $[\text{Ca}^{2+}]$ , see Eq. (1)) and stoichiometric equilibrium  
 169 constants. The concentrations of  $\text{Na}^+$ ,  $\text{Cl}^-$ , and  $\text{K}^+$  appear to have varied only slightly  
 170 over the last 100 Myr (see Section 2). In Appendix B, we examine the effects of changes  
 171 in  $[\text{Ca}^{2+}]$ ,  $[\text{Mg}^{2+}]$ , and  $[\text{SO}_4^{2-}]$  on the dissociation constants of carbonic acid ( $K_1^*$  and

172  $K_2^*$ ) and calcite solubility ( $K_{\text{spc}}^*$ ). We restrict our discussion to these constants for three  
 173 reasons. First,  $K_1^*$ ,  $K_2^*$ , and  $K_{\text{spc}}^*$  are by far the most important constants entering our  
 174 calculations. Second, the effect of changes in the remaining constants (e.g.,  $K_0$ ,  $K_w$ , ...) are  
 175 dwarfed by uncertainties in other parameters, including the reconstruction of the  
 176 major ion seawater composition itself. Third, it turns out that our results are not overly  
 177 sensitive to changes in  $K^*$ 's (see Section 5.3).

178 We compare all inferred major effects of  $[\text{Ca}^{2+}]$ ,  $[\text{Mg}^{2+}]$ , and  $[\text{SO}_4^{2-}]$  on  $K_1^*$ ,  $K_2^*$ ,  
 179 and  $K_{\text{spc}}^*$  to actual experimental data when deriving our  $K^*$  corrections. Reviewing the  
 180 experimental data requires some work (Appendix B) but provides the only rigorous  
 181 check on chemical seawater models (see note below). Given the various uncertainties  
 182 and limited available experimental data, we focus on data at 25°C to derive corrections  
 183 for the  $K^*$ 's.

184 In this paper, we denote thermodynamic and stoichiometric constants by  $K$  and  $K^*$ ,  
 185 respectively. Curly and square brackets denote activities (also  $a_i$ 's) and stoichiometric  
 186 concentrations, respectively. The equilibrium constants for the dissociation of carbonic  
 187 acid and calcite solubility may be written as:

$$K_1 = \frac{\{\text{HCO}_3^-\}\{\text{H}^+\}}{\{\text{CO}_2\} a_{\text{H}_2\text{O}}} \quad ; \quad K_1^* = \frac{[\text{HCO}_3^-][\text{H}^+]}{[\text{CO}_2]} \quad (4)$$

$$K_2 = \frac{\{\text{CO}_3^{2-}\}\{\text{H}^+\}}{\{\text{HCO}_3^-\}} \quad ; \quad K_2^* = \frac{[\text{CO}_3^{2-}][\text{H}^+]}{[\text{HCO}_3^-]} \quad (5)$$

$$K_{\text{spc}} = \{\text{Ca}^{2+}\}_{\text{sat}}\{\text{CO}_3^{2-}\}_{\text{sat}} \quad ; \quad K_{\text{spc}}^* = [\text{Ca}^{2+}]_{\text{sat}}[\text{CO}_3^{2-}]_{\text{sat}} \quad , \quad (6)$$

188 where 'sat' signifies saturation; for  $a_{\text{H}_2\text{O}}$ , see Appendix A. Introducing the total activity  
 189 coefficient  $\gamma_i$  of species  $i$ , with  $\{i\} = \gamma_i [i]$ , we can express the stoichiometric constants  
 190 by total activity coefficients and thermodynamic  $K$ 's, which are constants at given

191 temperature and pressure (i.e., do not depend on salinity, composition, etc.):

$$K_1^* = K_1 \frac{\gamma_{\text{CO}_2}}{\gamma_{\text{HCO}_3^-} \gamma_{\text{H}^+}} a_{\text{H}_2\text{O}} \quad (7)$$

$$K_2^* = K_2 \frac{\gamma_{\text{HCO}_3^-}}{\gamma_{\text{CO}_3^{2-}} \gamma_{\text{H}^+}} \quad (8)$$

$$K_{\text{spc}}^* = K_{\text{spc}} \frac{1}{\gamma_{\text{Ca}^{2+}} \gamma_{\text{CO}_3^{2-}}} ; \quad (9)$$

192 for  $\gamma_{\text{CO}_2}$ , see Appendix A. The above relationships are useful when illustrating the  
 193 effects of different major ion concentrations on stoichiometric equilibrium constants  
 194 (Appendix B). Furthermore, for the free activity coefficient we have  $\{i\} = \gamma_i^F [i]_F$ , and  
 195 hence  $\gamma_i/\gamma_i^F = [i]_F/[i]$ , where  $[i]$  is the total concentration (free + complexed). Note that  
 196 the  $K$ 's and  $K^*$ 's in Eqs. (7)-(9) should be expressed in the same units. For example,  $K$ 's  
 197 and  $K^*$ 's are often reported in units of  $\text{mol kg}^{-1}\text{-H}_2\text{O}$  (molality, concentration symbol  $m_i$ )  
 198 or  $\text{mol kg}^{-1}\text{-solution}$  (molamity, see Ramette, 2004), respectively. The conversion factor  
 199 from molality to molamity at standard seawater composition is  $w2s \simeq 1 - (0.001005 \times S)$ ,  
 200 where  $S$  is salinity (e.g., Millero, 1995).

### 201 3.1 Note on chemical models for seawater

202 For the present study, Millero and Schreiber's (1982) chemical model for seawater  
 203 (MS82 hereafter) turned out to be helpful (see Appendix B). The model is based on the  
 204 idea of ion pairing and builds on the work of Garrels and Thompson (1962) and others.  
 205 However, we emphasize that we do not advocate here the universal use of ion-pairing  
 206 models over, say, Pitzer models (though cf. Zeebe and Tyrrell, 2018) or other theoretical  
 207 approaches and do not argue for or against the theoretical basis of one particular model  
 208 (cf. May and Rowland, 2017). In this context, it is noteworthy that Pitzer models for  
 209 seawater actually include explicit ion pairing for some dissolved species and that more  
 210 recent work on ion pairing in the carbonic acid system (e.g. Stefánsson et al., 2013, 2014,  
 211 2017) is largely consistent with earlier work that formed the basis for various parameters

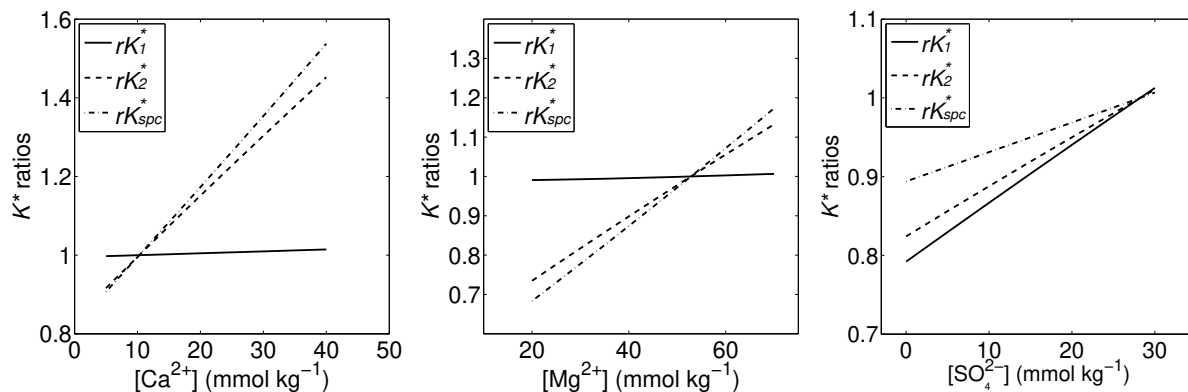


**Figure 3.:** Changes in  $K^*$  ratios relative to modern ( $rK^* = K^*/K_m^*$ ) predicted by the ion-pairing model (IPM) based on [Millero and Schreiber \(1982\)](#). Results are for standard seawater composition, except for changes in  $[\text{Ca}^{2+}]$ ,  $[\text{Mg}^{2+}]$ , and  $[\text{SO}_4^{2-}]$  as shown and in  $[\text{Na}^+]$  to maintain charge balance. Calculations also include changes in  $I$ , which affects free  $\gamma$ 's of ions,  $\gamma_{\text{CO}_2}$ ,  $a_{\text{H}_2\text{O}}$ , etc. (see [Appendix A](#)).

212 used in [Millero and Schreiber \(1982\)](#).

213 Nevertheless, chemical models for seawater still have large uncertainties and the  
 214 data on which they are based are in some cases insufficient, inconsistent, or lacking  
 215 altogether (discussed in [Appendix B](#)). To improve the situation for studies such as the  
 216 present one, we advocate the experimental determination of stoichiometric equilibrium  
 217 constants for the particular major ion compositions of past oceans, i.e., at minimum  
 218 including variations of the concentrations of  $\text{Ca}^{2+}$ ,  $\text{Mg}^{2+}$ , and  $\text{SO}_4^{2-}$  over relevant  
 219 ranges (e.g., [Horita et al., 2002](#)). The currently available data for  $K_1^*$ ,  $K_2^*$ , and  $K_{\text{spc}}^*$  are  
 220 examined in [Appendix B](#).

### 221 3.2 Summary: Equilibrium constants

222 As described in [Appendix B](#), the trends expected from Eqs. (7)-(9) for the effects  
 223 of calcium, magnesium, and sulfate on stoichiometric equilibrium constants and activity  
 224 coefficients are consistent with data from various laboratory measurements. Also, for the  
 225 present purpose, the trends predicted by the ion-pairing model (IPM, based on [Millero  
 226 and Schreiber, 1982](#)) are sufficiently close to the observed trends (Figs. [B.1-B.3](#), [B.5](#)).  
 227 Importantly, absolute values predicted by the IPM are secondary for our approach. As

228 in Tyrrell and Zeebe (2004), we use established standard stoichiometric  $K^*$ 's below  
 229 (experimentally determined using modern seawater media as standard states) and only  
 230 apply relative changes to  $K^*$ 's as functions of  $[\text{Ca}^{2+}]$ ,  $[\text{Mg}^{2+}]$ , and  $[\text{SO}_4^{2-}]$  ( $x_j$ 's for short,  
 231 where  $j = 1, 2, 3$ ). In the following, we will use the IPM trends to correct  $K^*$ 's for past  
 232 changes in seawater composition. Our calculations also include changes in  $[\text{Na}^+]$  and  $I$ ,  
 233 which affects free activity coefficients of ionic species,  $\gamma_{\text{CO}_2}$ ,  $a_{\text{H}_2\text{O}}$ , etc. (see Appendix A).

234 For relevant ranges of  $x_j$  changes in the past (see Section 2), the relative changes in  
 235  $K^*$ 's (or  $K^*$  ratios) predicted by the IPM are virtually linear when  $x_j$ 's vary individually  
 236 (Fig. 3). Even when  $x_j$ 's vary simultaneously,  $K^*$  ratios remain very close to linear (see  
 237 Appendix C), allowing a simple linear parameterization to a very good approximation  
 238 (Ben-Yaakov and Goldhaber, 1973; Tyrrell and Zeebe, 2004), although with new  
 239 sensitivity parameters  $s_{ij}$ :

$$K_i^*/K_{i,m}^* = 1 + \sum_{j=1}^3 s_{ij} (x_j/x_{j,m} - 1) \quad (10)$$

240 where  $m = \text{modern}$ ,  $i = 1, 2, \text{spec}$ , and  $x_j$  refers to  $[\text{Ca}^{2+}]$ ,  $[\text{Mg}^{2+}]$ , and  $[\text{SO}_4^{2-}]$ . The  $s_{ij}$   
 241 were obtained from linear fits to the IPM results shown in Fig. 3 for maintaining charge  
 242 balance via  $[\text{Na}^+]$  adjustment (see Table 2). Parameters for constant ionic strength  
 243 are given in Appendix D. The computational effort for our approach is minimal and  
 244 well-suited for easy  $K^*$ -corrections in numerical models as well as observational studies,  
 245 at an accuracy appropriate for seawater carbonate chemistry and  $\text{CO}_2$  reconstructions  
 246 on multi-million year time scales.

247 Given past changes in major ion composition (Fig. 1a) and the effects of  $[\text{Ca}^{2+}]$ ,  
 248  $[\text{Mg}^{2+}]$ , and  $[\text{SO}_4^{2-}]$  on  $K^*$ 's as estimated above (Fig. 3), corrections for past stoichiometric  
 249 equilibrium constants can then be calculated (Eq. (10), Fig. 4). These  $K^*$  ratios will be  
 250 used below to calculate carbonate chemistry parameters over time.

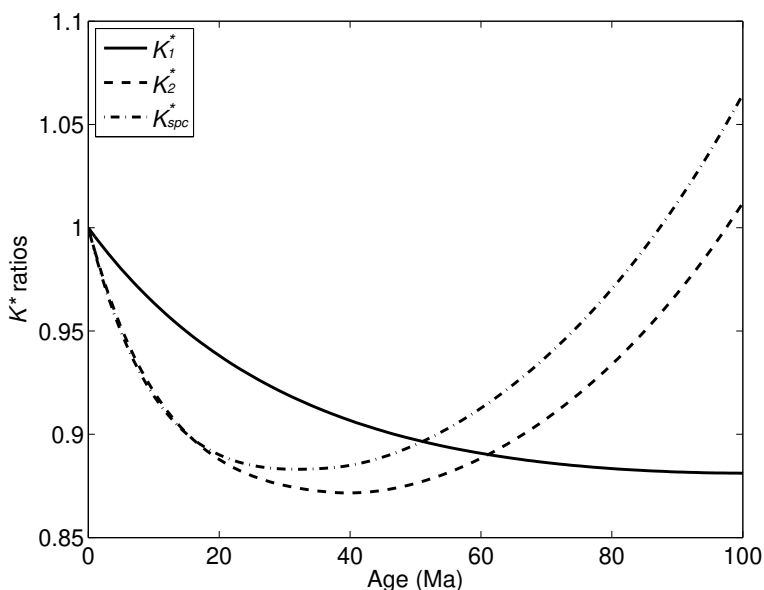


**Figure 4.:** Past changes in  $K^*$ 's (or  $K^*$  ratios, Eq. (10)) estimated from reconstructed changes in  $[\text{Ca}^{2+}]$ ,  $[\text{Mg}^{2+}]$ , and  $[\text{SO}_4^{2-}]$  (Fig. 1a) and effects on  $K^*$ 's (Fig. 3).  $[\text{Na}^+]$  was adjusted to maintain charge balance.

**Table 2.:** Sensitivity parameters  $s_{ij} \times 10^3$  (dimensionless) for Eq. (10) with  $[\text{Na}^+]$  adjustment to maintain charge balance.

	$K_1^*$	$K_2^*$	$K_{\text{spc}}^*$
$\text{Ca}^{2+}$	5	157	185
$\text{Mg}^{2+}$	17	420	518
$\text{SO}_4^{2-}$	208	176	106

## 4 Long-term Trends in Ocean Carbonate Chemistry over the last 100 Myr

From the history of  $[\text{Ca}^{2+}]$  (Fig. 1a) and seawater calcite saturation state (Tyrrell and Zeebe, 2004), we estimate the long-term evolution of surface  $[\text{CO}_3^{2-}]$  over the last 100 Myr (Fig. 5a). It turns out that our new surface  $[\text{CO}_3^{2-}]$  is very similar to that published 14 years ago (Tyrrell and Zeebe, 2004), except being slightly higher at 100 Ma. The reason for the similarity is that changes due to updates in equilibrium constants (raising past  $[\text{CO}_3^{2-}]$ ) are partly compensated for by higher reconstructed  $[\text{Ca}^{2+}]$  (lowering past

259  $[\text{CO}_3^{2-}]$ ). Combining  $[\text{CO}_3^{2-}]$  with one other carbonate chemistry parameter (plus  $T, S$   
 260 estimates) allows computation of the remaining carbonate chemistry parameters.

261 We emphasize that our reconstructions based on  $[\text{CO}_3^{2-}]$  are inherently long-term  
 262 trend estimates over  $\gtrsim 10$ -Myr intervals. We do not resolve events and aberrations such  
 263 as the MECO, the hyperthermals (PETM, ELMO, . . .), etc. Likewise, changes in trends  
 264 on time scales  $\lesssim 10$  Myr are not resolved, including those during the early Paleogene,  
 265 which warrant a more detailed analysis (e.g., Komar et al., 2013). One exception is  
 266 the Middle Miocene Climatic Optimum (MMCO,  $\sim 17$ -15 Ma), which we briefly discuss  
 267 below in the context of boron isotope data.

#### 268 4.1 Long-term trends from $[\text{CO}_3^{2-}]$ and atmospheric $\text{CO}_2$

269 In this section we use independent  $p\text{CO}_2$  estimates either from GEOCARB  
 270 modeling or from alkenones as the second parameter (Fig. 5). Estimates for  $T$  and  
 271  $S$  used for the GEOCARB scenario were unchanged from Tyrrell and Zeebe (2004),  
 272 while  $T$  information for the alkenone scenario were directly taken from each of the  
 273 published alkenone data sets without smoothing;  $S$  was assumed constant (cf. also  
 274 [www.p-co2.org](http://www.p-co2.org) and Rae (2018)). The modern surface  $[\text{CO}_3^{2-}]$  was set to  $200 \mu\text{mol kg}^{-1}$   
 275 for the GEOCARB scenario, corresponding to preindustrial values of  $p\text{CO}_2 = 280 \mu\text{atm}$   
 276 and  $p\text{H} = 8.18$  on the total scale (Zeebe and Wolf-Gladrow, 2001) at a global mean sea  
 277 surface temperature of  $T \simeq 15^\circ\text{C}$ . For the alkenone scenario, modern surface  $[\text{CO}_3^{2-}]$   
 278 was set to  $250 \mu\text{mol kg}^{-1}$ , more representative for modern sea surface temperatures  
 279 of  $T \gtrsim 20^\circ\text{C}$  at the latitudinal site distribution of the alkenone studies included here  
 280 (Fig. 5a).

281 Using our  $[\text{CO}_3^{2-}]$  and the  $p\text{CO}_2$  reconstructions, surface ocean DIC (total dissolved  
 282 inorganic carbon), TA (total alkalinity), and  $p\text{H}$  can be calculated (Fig. 5). At present,  
 283 no independent reliable proxies exist for DIC and TA. However, we can use surface  
 284 ocean  $p\text{H}$  estimates from stable boron isotope records ( $\delta^{11}\text{B}$ ) as an independent check

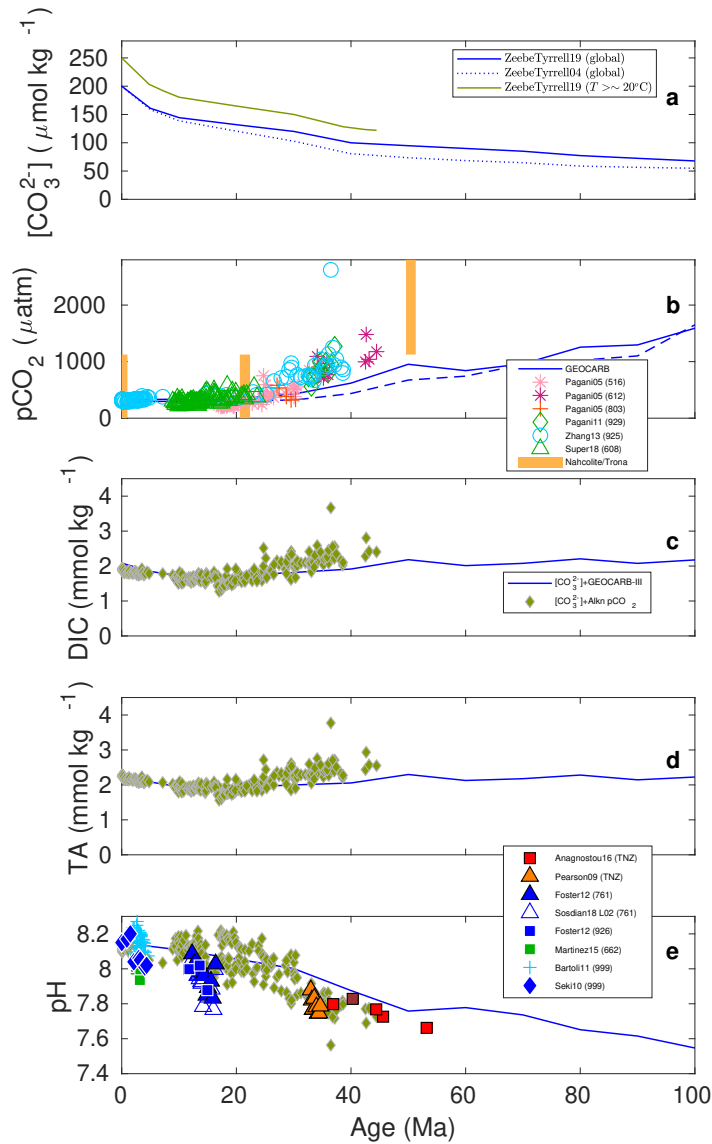


**Figure 5.** Estimates of carbonate chemistry parameters from (a) surface ocean  $[\text{CO}_3^{2-}]$  (this study & TZo4) and (b)  $p\text{CO}_2$ . Independent  $p\text{CO}_2$  estimates are from GEOCARB-III and GEOCARBSULF (dashed) (Berner and Kothavala, 2001; Berner, 2006, 2008) and alkenones (e.g., Pagani et al., 2005; Pagani et al., 2011; Zhang et al., 2013; Super et al., 2018). Bars: ranges from mineral-phase equilibria (Nahcolite/Trona) (Lowenstein, 2006). The GEOCARB and alkenone scenarios use  $[\text{CO}_3^{2-}]$  corresponding to global modern mean  $T \approx 15^\circ\text{C}$  and  $T \gtrsim 20^\circ\text{C}$  (see (a)). The results for  $p\text{H}$  (blue line, olive diamonds in (e)) may be compared to independent boron-based  $p\text{H}$  estimates (see legend) (e.g., Anagnostou et al., 2016; Pearson et al., 2009; Foster et al., 2012; Sosdian et al., 2018; Martinez-Botí et al., 2015; Bartoli et al., 2011; Seki et al., 2010), cf. also [www.p-co2.org](http://www.p-co2.org) and Rae (2018). Our results are available at [www.soest.hawaii.edu/oceanography/faculty/zeebe\\_files/ZT19.html](http://www.soest.hawaii.edu/oceanography/faculty/zeebe_files/ZT19.html).

285 on the  $[\text{CO}_3^{2-}] + p\text{CO}_2$  combination (Fig. 5e). Again, note that the GEOCARB time step  
 286 is of order 10 Myr and hence does not resolve events (MECO, PETM, ELMO, etc.) and  
 287 changes in trends  $\lesssim 10$  Myr, say, during the early Paleogene (e.g., Komar et al., 2013).



288 Overall, the trends in CO<sub>2</sub> system parameters across the Cenozoic appear consistent.  
 289 For example, consistency for *p*H may be quantified by calculating the difference ( $\Delta p$ H)  
 290 between *p*H values derived from the [CO<sub>3</sub><sup>2-</sup>]+alkenone *p*CO<sub>2</sub> combination vs. *p*H values  
 291 derived from boron (Fig. 5e). Using a series of 1-Myr bins in which the two data sets  
 292 overlap ( $N = 16$ ), the average absolute  $\Delta p$ H over the last 45 Myr is  $\sim 0.07$  *p*H units (much  
 293 larger, i.e.,  $\sim 0.12$  *p*H units if we assumed constant, modern [CO<sub>3</sub><sup>2-</sup>]). For comparison,  
 294 the reported errors on boron-based *p*H for records younger than  $\sim 20$  Ma, are typically  
 295 0.02-0.07 units (Martínez-Botí et al., 2015; Bartoli et al., 2011; Seki et al., 2010) and  
 296 0.05-0.07 units for the Eocene records (Anagnostou et al., 2016; Pearson et al., 2009)  
 297 but can be larger if uncertainties in seawater  $\delta^{11}\text{B}$  are fully propagated. Importantly,  
 298 however,  $\Delta p$ H can be caused not only by errors but also by natural short-term and/or  
 299 spatial environmental variability, e.g., when combination-*p*H and/or boron-*p*H values are  
 300 not from exactly the same times or cores. To illustrate this point, we have also calculated  
 301 the average standard deviation ( $\bar{\sigma}$ ) of independent boron-*p*H values in the same 1-Myr  
 302 bin, for bins containing more than one value ( $N = 12$ ), which yields  $\bar{\sigma} \approx 0.04$  *p*H units.

303 Pagani et al. (2011) and Zhang et al. (2013) both reported one rather high  
 304 alkenone-*p*CO<sub>2</sub> value  $> 2,500$   $\mu\text{atm}$  at  $\sim 36$  Ma (Fig. 5b) from the same core interval at  
 305 ODP Site 925, only Zhang et al. used a different age model and parameters to calculate  
 306 *p*CO<sub>2</sub>. Hence, only one value should be displayed in compilations, not both. The reason  
 307 for the unusually high value remains unclear but is unlikely to be a measurement error.

308 When comparing CO<sub>2</sub> system parameters, one needs to be careful in selecting truly  
 309 independent variables to avoid circularity. For example, the *p*CO<sub>2</sub> obtained from  $\delta^{11}\text{B}$   
 310 records is a derived variable because it is based on *p*H, which requires one additional  
 311 parameter and is therefore not an independent quantity in the context of carbonate  
 312 chemistry. In fact, most boron-based studies make assumptions about past DIC, TA,  
 313 or [CO<sub>3</sub><sup>2-</sup>] to derive *p*CO<sub>2</sub>. Hence if one were to use  $\delta^{11}\text{B}$ -derived *p*CO<sub>2</sub> as the second

parameter, one would essentially recover DIC, TA, or  $[\text{CO}_3^{2-}]$  values as assumed in the first place, which is circular. However, we may use our  $[\text{CO}_3^{2-}]$  plus  $\delta^{11}\text{B}$ - $p\text{H}$  to derive  $p\text{CO}_2$  and compare our results to other  $p\text{CO}_2$  estimates (Section 4.2).

#### 4.2 Long-term trends from $[\text{CO}_3^{2-}]$ and $p\text{H}$

In this section we use our  $[\text{CO}_3^{2-}]$  together with independent  $p\text{H}$  estimates from  $\delta^{11}\text{B}$  records as the second parameter (Fig. 6). Temperature estimates for the  $p\text{H}$  scenarios were taken from the published  $\delta^{11}\text{B}$  data sets. For the  $p\text{H}$  scenario, modern surface  $[\text{CO}_3^{2-}]$  was set to  $280 \mu\text{mol kg}^{-1}$ , more representative for modern sea surface temperatures of  $T \gtrsim 25^\circ\text{C}$  at the latitudinal site distribution of the boron studies included here (Fig. 6a). **As explained in Section 3, compared to the effects of seawater composition on  $K_1^*$ ,  $K_2^*$ ,  $K_{\text{sp}}^*$ , and various other uncertainties, effects of changes in the boric acid dissociation constant  $K_B^*$  are small. Moreover, for our parameter combinations,  $K_B^*$  only affects TA estimates. For instance, changing  $K_B^*$  by 20%, yields  $\Delta\text{TA} \simeq 10 \mu\text{mol kg}^{-1}$ .** The Cenozoic long-term evolution of boron-derived  $p\text{H}$  appears consistent with  $p\text{H}$  from our  $[\text{CO}_3^{2-}]$  and GEOCARB  $p\text{CO}_2$  (dashed line, Fig. 6b), although boron- $p\text{H}$  is generally lower in the past, particularly during intervals such as the Middle Miocene Climatic Optimum (MMCO,  $\sim 17$ -15 Ma) and the Eocene-Oligocene Transition (EOT), which are not resolved in GEOCARB. Correspondingly,  $p\text{CO}_2$  derived from our  $[\text{CO}_3^{2-}]$  and  $\delta^{11}\text{B}$ - $p\text{H}$  is generally higher than the GEOCARB estimates (Fig. 6e).

However, note that our reconstructions for intervals such as the MMCO should be taken with caution because they combine one inherent long-term (our  $[\text{CO}_3^{2-}]$ ) and one short-term parameter (boron- $p\text{H}$ ) during relatively fast Earth system changes. Short-term variations in  $[\text{CO}_3^{2-}]$  during the MMCO are of course possible, if not likely, and because they are not resolved, bias our reconstructions (potentially overestimating  $p\text{CO}_2$  for the low- $p\text{H}$  data). Also note that [Sosdian et al. \(2018\)](#) provided various additional  $p\text{H}$  scenarios for ODP Site 761 (cf. [Foster et al., 2012](#)). Thus we have included one

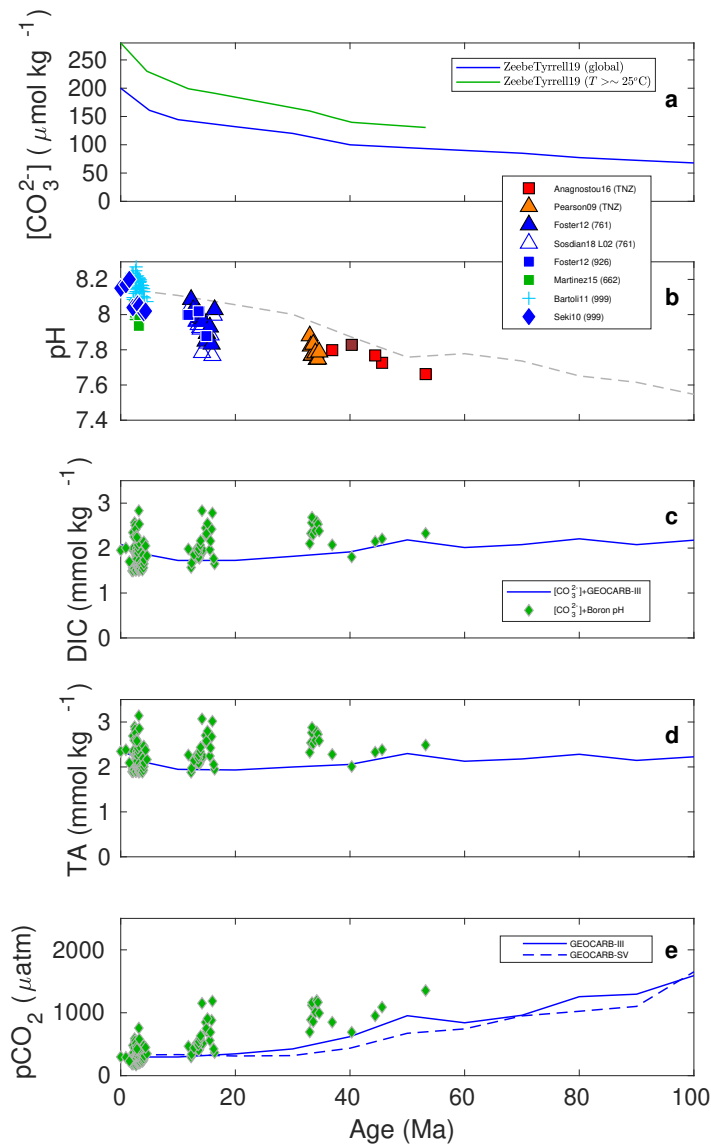


**Figure 6.** Estimates of carbonate chemistry parameters from (a) surface ocean  $[\text{CO}_3^{2-}]$  (this study) and (b) independent  $p\text{H}$  estimates from boron-based studies (symbols, cf. also [www.p-co2.org](http://www.p-co2.org) and [Rae \(2018\)](#)). The  $p\text{H}$  scenarios use surface  $[\text{CO}_3^{2-}]$  corresponding to  $T \gtrsim 25^\circ\text{C}$  (see (a)). In (e), GEOCARB-SV: GEOCARBSULF model including volcanic rock weathering. For references, see Fig. 5. Dashed line in (b) shows  $p\text{H}$  from our  $[\text{CO}_3^{2-}]$  and GEOCARB- $p\text{CO}_2$  for comparison. Our results are available at [www.soest.hawaii.edu/oceanography/faculty/zeebe\\_files/ZT19.html](http://www.soest.hawaii.edu/oceanography/faculty/zeebe_files/ZT19.html).

340 “high- $p\text{H}$ ” MMCO scenario ([Foster et al., 2012](#)) and one of the “low- $p\text{H}$ ” scenario,  
 341 labeled “Soslidian18 Lo2” (Figs. 5e and 6b), which uses [Lemarchand et al. \(2002\)](#)’s  
 342 seawater  $\delta^{11}\text{B}$  ([Soslidian et al., 2018](#)).

## 5 Discussion

### 5.1 Past DIC and TA inventories

Our reconstructions suggest that long-term DIC and TA were similar to modern values across the past 100 Myr, regardless of whether  $p\text{CO}_2$  or  $p\text{H}$  is used as the second parameter with our  $[\text{CO}_3^{2-}]$  (Figs. 5 and 6). This may appear surprising, given that Cenozoic  $p\text{CO}_2$  was mostly higher than modern, which, everything else being the same, would suggest elevated DIC (see Zeebe and Wolf-Gladrow, 2001). However, the relatively low DIC despite high  $p\text{CO}_2$  is a direct consequence of higher  $[\text{Ca}^{2+}]$  in the past, which leads to lower  $[\text{CO}_3^{2-}]$ , given moderate changes in carbonate saturation (Fig. 5a). Briefly, the effect of elevated past  $\text{CO}_2$  levels on DIC was largely compensated for by lower  $[\text{CO}_3^{2-}]$ .

### 5.2 CCD records

As discussed in detail in TZ04, records of the calcite compensation depth (CCD) indicate that the ocean's calcite saturation state ( $\Omega$ ) has not varied dramatically over the past 100 Myr. Nevertheless, to account for changes in whole-ocean saturation, TZ04 used a smoothed global CCD curve (Fig. 7), which should reflect changes in  $\Omega$ . In turn, changes in  $\Omega$  affect  $[\text{CO}_3^{2-}]$  via Eq. (1) (see Appendix E), but to what extent? The effect of CCD changes on our calculated  $[\text{CO}_3^{2-}]$  may be illustrated by replacing the global CCD curve by reconstructions for the equatorial Pacific CCD (Pälike et al., 2012). This test merely serves as an illustration; we emphasize that the equatorial Pacific CCD is not a substitute for the global CCD. Nevertheless, the effect is small (Fig. 7), suggesting that our  $[\text{CO}_3^{2-}]$  reconstruction is insensitive to details of  $\Omega$ /CCD changes across the Cenozoic.

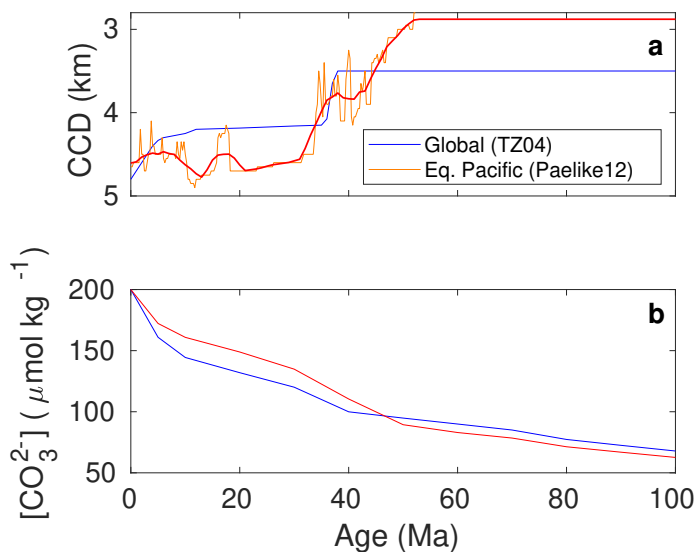


**Figure 7.:** Effect of (a) calcite compensation depth (CCD) on (b)  $[\text{CO}_3^{2-}]$  via saturation state  $\Omega$  (see text). Default calculations use changes in global CCD after TZ04 (blue lines). Red lines illustrate the effect on  $[\text{CO}_3^{2-}]$  if reconstructions for the equatorial Pacific CCD were used instead (Pälike et al., 2012). We emphasize, however, that the equatorial Pacific CCD is not a substitute for the global CCD. Because our  $[\text{CO}_3^{2-}]$  proxy is inherently long-term (see text), a smoothed curve (thick red line in (a)) was used. To allow comparison with the global CCD record (blue curve in (a)), the red curve was set constant between 50 and 100 Ma.

### 5.3 Error propagation

Uncertainties in our reconstructions may be evaluated by assigning errors to important parameters and propagating those through the calculations. Important parameters that affect our results include changes in temperature ( $T$ ), salinity ( $S$ ), major ion concentrations, sensitivity parameters for  $K^*$  corrections ( $s_{ij}$ ), and the ocean's calcite saturation state ( $\Omega$ ), as inferred from CCD changes. Additional parameters enter the calculations but not all are critical. For instance, the total boron concentration in seawater makes no difference for  $p\text{H}$ , when calculated from  $[\text{CO}_3^{2-}]$  and  $[\text{CO}_2]$ , although it does affect TA (Zeebe and Wolf-Gladrow, 2001). In the following, we focus on the parameters listed above, which are most critical for our reconstructed  $p\text{H}$  and  $p\text{CO}_2$ . Importantly, our error propagation provides uncertainty estimates for our results based on given, assigned parameter errors. The assigned errors themselves are somewhat arbitrary and mostly chosen rather generously. For example, an assigned maximum

379 temperature error of  $\pm 5$  K at 100 Ma (see below) is most likely at the upper end of  
 380 realistic values. Hence our emphasis is on providing what-if scenarios, rather than  
 381 precise parameter errors.

### 382 5.3.1 Individual error propagation

383 To illustrate the effect of uncertainties in individual parameters on our results, in  
 384 this section we propagate errors separately for two scenarios. First, we calculate  $p\text{H}$  from  
 385 our  $[\text{CO}_3^{2-}]$  (including errors) and GEOCARB  $p\text{CO}_2$  (Fig. 8, middle column). Second,  
 386 we calculate  $p\text{CO}_2$  from our  $[\text{CO}_3^{2-}]$  (including errors) and the standard  $p\text{H}$  result of the  
 387 first (GEOCARB) scenario (Fig. 8, right column). This allows for easy inspection of  
 388  $p\text{H}$  and  $p\text{CO}_2$  uncertainties for related scenarios. The emphasis here is on estimating  
 389 maximum uncertainties from individual parameters and will involve some non-standard  
 390 assumptions about errors.

391 Errors in  $T$ ,  $S$ , and CCD were assumed to grow linearly with time in the past so  
 392 that the maximum error was assigned at 100 Ma (variables with subscript label ‘100’ in  
 393 Fig. 8).  $T$  and  $S$  affect the various equilibrium constants, with an opposite net effect on  
 394 our calculated  $p\text{CO}_2$ . Hence we combined an increase in  $T$  with a drop in  $S$  and vice  
 395 versa (Fig. 8, 1st row). The major ion concentrations ( $[\text{Ca}^{2+}]$ ,  $[\text{Mg}^{2+}]$ ,  $[\text{SO}_4^{2-}]$ ) were varied  
 396 within their estimated standard error envelopes (see Fig. 1a); **for uncertainties resulting**  
 397 **from the value used for  $[\text{Ca}^{2+}] \times [\text{SO}_4^{2-}]$ , see Section 5.3.2.** Sensitivity parameters  
 398 for  $K^*$  corrections ( $s_{ij}$ ) were assigned a constant error of  $\pm 100\%$ , while  $\Omega$  was varied  
 399 corresponding to an assigned maximum CCD error of  $\pm 1$  km at 100 Ma.

400 The propagated uncertainty for  $[\text{CO}_3^{2-}]$  and  $p\text{H}$  is moderate; for  $p\text{CO}_2$  it is more  
 401 significant (ca.  $\pm 300$   $\mu\text{atm}$ ). However, note that the assigned maximum parameter  
 402 errors at 100 Ma of  $T \pm 5$  K and  $S \mp 3$  are rather large. Varying  $[\text{Ca}^{2+}]$ ,  $[\text{Mg}^{2+}]$ , and  
 403  $[\text{SO}_4^{2-}]$  within their estimated error envelopes (Fig. 1a) has a small effect on  $[\text{CO}_3^{2-}]$  and  
 404  $p\text{H}$ , and a slightly larger impact on  $p\text{CO}_2$ , ca.  $\pm 250$   $\mu\text{atm}$  (Fig. 8, 2nd row). Large

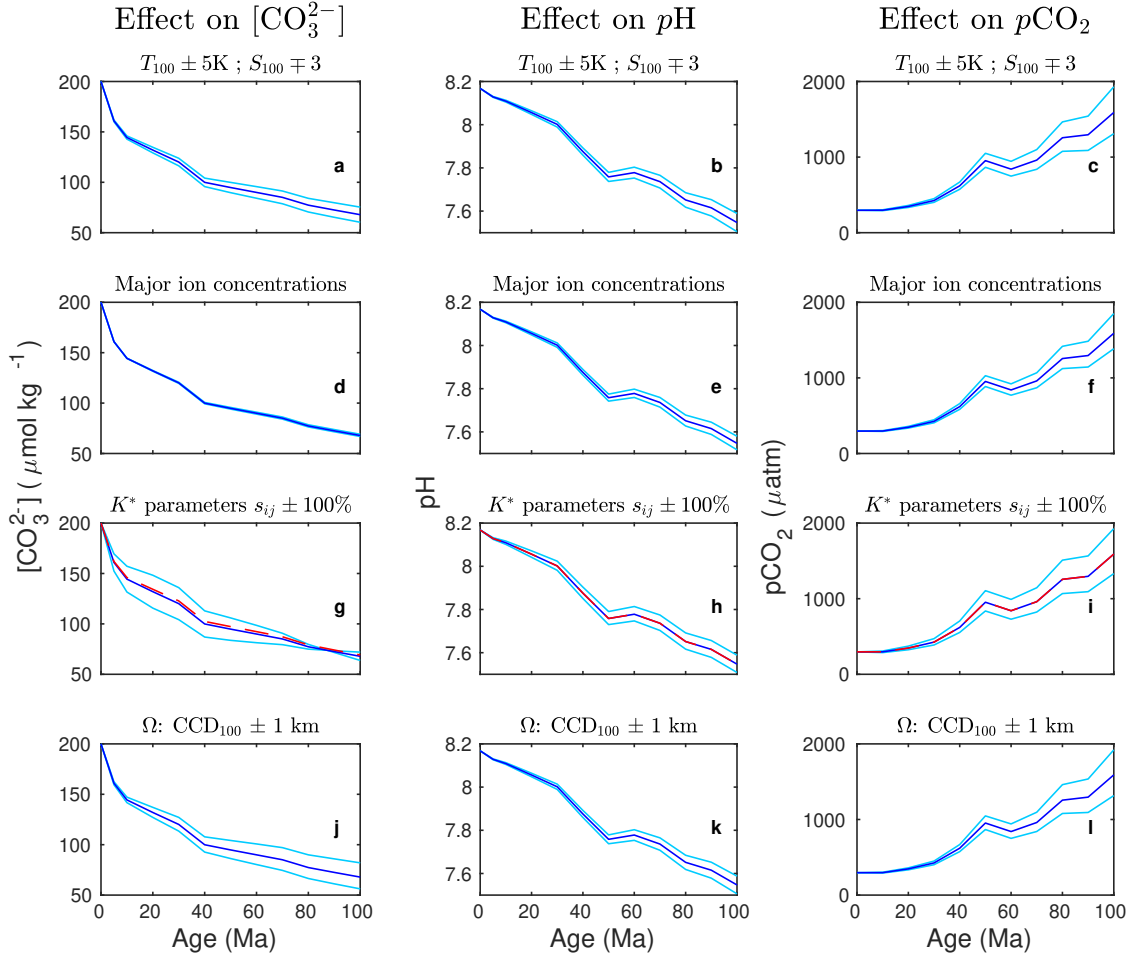


**Figure 8:** Individual error propagation of critical parameters for  $[\text{CO}_3^{2-}]$  (column 1),  $\text{pH}$  (column 2), and  $\text{pCO}_2$  (column 3) reconstructions. Dark blue: standard scenarios, light blue: upper and lower uncertainty bounds for assigned parameter errors (see text for details). Red dashed line (3rd row):  $\gamma_{\text{CO}_3^{2-}}^F$  in IPM changed from 0.2 (default) to 0.3 (cf. Section B.1).

405 changes in sensitivity parameters  $s_{ij}$  for  $K^*$  corrections by  $\pm 100\%$  (factor 0 and 2) only  
 406 have a moderate effect throughout (Fig. 8, 3rd row). As a result, using no corrections  
 407 at all ( $0 \times s_{ij}$  means modern  $K^*$ 's) would result in  $\text{pCO}_2$  values  $\sim 250 \mu\text{atm}$  too low at  
 408 100 Ma for the example shown (and  $\sim 100 \mu\text{atm}$  too low at 50 Ma). Changing  $\gamma_{\text{CO}_3^{2-}}^F$  from  
 409 0.2 (default) to 0.3 in the IPM has virtually no effect on the results (cf. Section B.1).  
 410 Variations in  $\Omega$  (via CCD) have a noticeable effect on  $[\text{CO}_3^{2-}]$  and  $\text{pCO}_2$  (ca.  $\pm 300 \mu\text{atm}$   
 411 at 100 Ma), although the assigned maximum CCD error of  $\pm 1 \text{ km}$  at 100 Ma is probably

412 quite large (Fig. 8, 4th row).

### 413 5.3.2 Errors from assumed $[\text{Ca}^{2+}] \times [\text{SO}_4^{2-}]$ value

414 The standard values for  $[\text{Ca}^{2+}]$  and  $[\text{SO}_4^{2-}]$  vs. time compiled in Fig. 1a were derived  
 415 by the fluid inclusion studies assuming constant, modern  $[\text{Ca}^{2+}] \times [\text{SO}_4^{2-}]$  in the past.  
 416 Additional  $\text{Ca}^{2+}$  and  $\text{SO}_4^{2-}$  concentrations were provided by these studies for different  
 417 values of  $[\text{Ca}^{2+}] \times [\text{SO}_4^{2-}]$ . For example, using 1.0, 0.5, and 1.5 times the modern  
 418  $[\text{Ca}^{2+}] \times [\text{SO}_4^{2-}]$  value results in  $[\text{Ca}^{2+}]$  and  $[\text{SO}_4^{2-}]$  of  $16_{-5}^{+4}$  and  $19_{-5}^{+4}$  mmol  $\text{kg}^{-1}\text{-H}_2\text{O}$  in  
 419 the Eocene at  $\sim 37$  Ma (Horita et al., 2002) and  $26_{-6}^{+2}$  and  $14_{-6}^{+2}$  mmol  $\text{kg}^{-1}\text{-H}_2\text{O}$  in the  
 420 Cretaceous at  $\sim 100$  Ma (Timofeeff et al., 2006). These uncertainty ranges are similar  
 421 to the assigned parameter errors for  $[\text{Ca}^{2+}]$  and  $[\text{SO}_4^{2-}]$  in our Monte Carlo simulations  
 422 ( $\pm 5$  mmol  $\text{kg}^{-1}$ , see Table 3 below) and are hence covered by our Monte Carlo error  
 423 propagation (Section 5.3.3). Such parameter errors affect the equilibrium constants  
 424 via  $x_j$ 's (Eq. (10)) but not the sensitivity parameters  $s_{ij}$ , which are derived taking  
 425 into account charge balance via  $[\text{Na}^+]$  adjustment (Table 2) or constant ionic strength  
 426 (Appendix D) for each combination of the  $x_j$ 's within their relevant ranges (Fig. C.1).  
 427 Larger errors in  $[\text{Ca}^{2+}]$  and  $[\text{SO}_4^{2-}]$  do increase the uncertainties in the reconstructed  $\text{Na}^+$   
 428 concentration and flux based on charge balance (Fig. 2). Finally, we note that the Mg/Ca  
 429 ratio of seawater,  $(\text{Mg}/\text{Ca})_{sw}$ , as derived by fluid inclusion studies based on modern  
 430  $[\text{Ca}^{2+}] \times [\text{SO}_4^{2-}]$  is consistent with independent estimates of  $(\text{Mg}/\text{Ca})_{sw}$  (see Fig. 1b and  
 431 discussion in Horita et al. (2002)). Alternatively, instead of constant  $[\text{Ca}^{2+}] \times [\text{SO}_4^{2-}]$ ,  
 432 perhaps one could assume that past changes in  $[\text{Ca}^{2+}]$  were accompanied by equivalent  
 433 changes in  $[\text{SO}_4^{2-}]$  to maintain charge balance. However, this would lead to different  
 434  $(\text{Mg}/\text{Ca})_{sw}$  ratios in the past and leave changes in  $[\text{Mg}^{2+}]$  essentially unbalanced (Fig. 1).

435



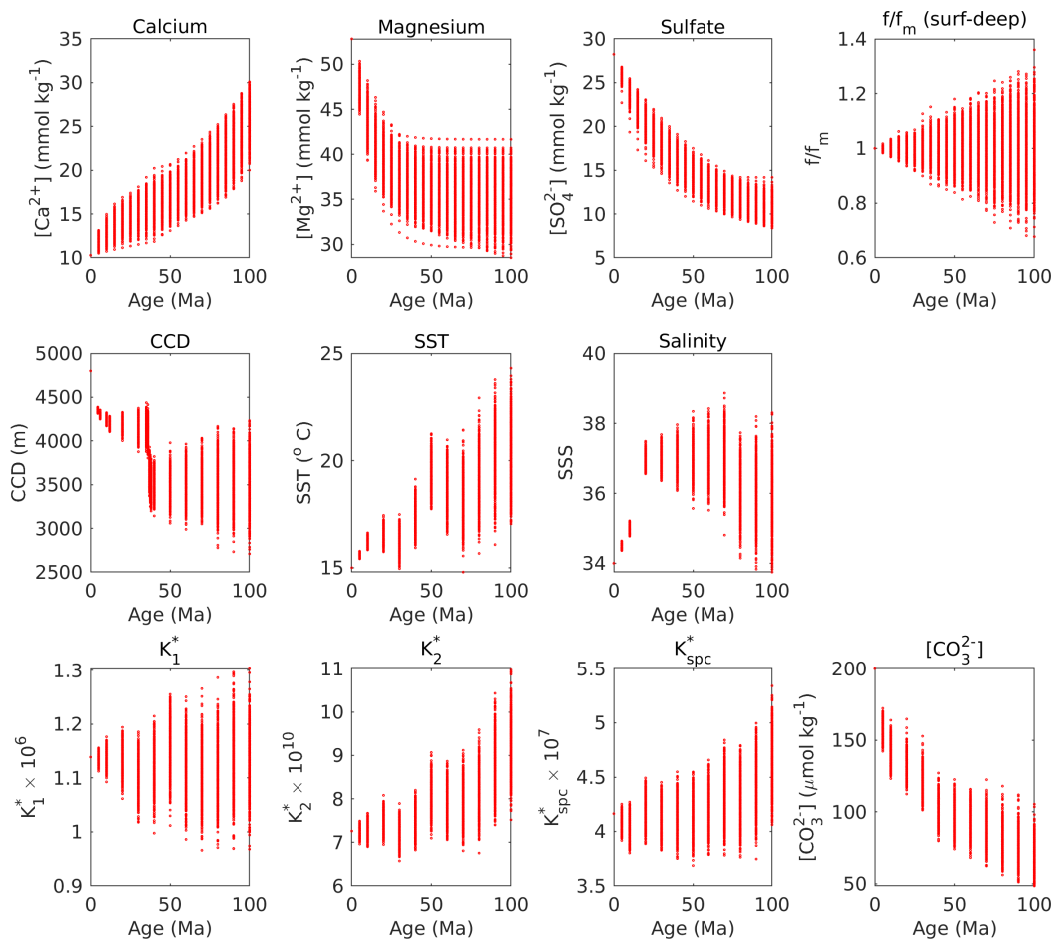


**Figure 9.:** Results of Monte Carlo simulation. Parameter variations were applied at 5 to 10 Myr time steps, see text. Each dot represents the result of a single run at that time step. *Sea surface temperature (SST) after TZO<sub>4</sub>. Salinity from GEOCARB-III was used here for direct comparison with TZO<sub>4</sub> but may be replaced by more recent estimates (the effect is small).*

### 436 5.3.3 Monte Carlo error propagation

437 In this section, we follow standard practice and assume that all errors are random  
 438 and normally distributed (Central Limit Theorem), but note that in reality systematic  
 439 errors are also possible. The effect of the allocated errors on the uncertainty of the  
 440 results was determined using a Monte Carlo approach in which the entire calculation  
 441 procedure was executed 1,000 times with randomly different errors (Fig. 9, Table 3).  
 442 The uncertainties of the results are reported as  $\pm 2\sigma$  (twice the standard deviation of

443 1,000 results).

444 For  $[\text{Ca}^{2+}]$ ,  $[\text{Mg}^{2+}]$ , and  $[\text{SO}_4^{2-}]$  we added normally distributed errors to the data  
 445 with standard deviation equal to half of the distance to the envelope (95% of values in a  
 446 normal distribution are within  $\pm 2\sigma$  of the mean). Errors in  $[\text{Ca}^{2+}]$ ,  $[\text{Mg}^{2+}]$ , and  $[\text{SO}_4^{2-}]$   
 447 were applied regardless of age (Table 3), after which an exponential function was fit to  
 448 data+errors. This leads to larger variations in the fit function in the past because its  
 449 value is fixed to the modern concentration at  $t = 0$  Ma (Fig. 9). To account for possible  
 450 changes in the surface-to-deep  $[\text{CO}_3^{2-}]$  gradient in the past (actually ratio), we randomly  
 451 varied the ratio  $f/f_m$ , with  $[\text{CO}_3^{2-}]_s = f[\text{CO}_3^{2-}]_d$  and indices  $s$ ,  $d$ , and  $m$  refer to surface,  
 452 deep, and modern. For details and a comprehensive discussion of the surface-to-deep  
 453 ratio, see Appendix of TZo4. As above, errors in CCD, temperature, salinity, and  
 454  $f/f_m$  were assumed to grow linearly with time in the past. Variations in major ion  
 455 composition, temperature, and salinity then lead to variations in the stoichiometric  
 456 equilibrium constants  $K^*$ , which depend on these parameters (Fig. 9). Finally, the  
 457 propagated uncertainty in  $[\text{CO}_3^{2-}]$  from the combined errors of all parameters can be  
 458 calculated (Fig. 9). For example, at 100 Ma,  $2\sigma \simeq 18 \mu\text{mol kg}^{-1}$  and hence we estimate  
 459 that  $[\text{CO}_3^{2-}]$  was about 2.3 to 4-fold lower at 100 Ma ( $\sim 68 \pm 18 \mu\text{mol kg}^{-1}$  for a modern  
 460 value of  $200 \mu\text{mol kg}^{-1}$ ).

Table 3.: Assigned parameter errors ( $2\sigma$ ) for the Monte Carlo simulation.

$[\text{Ca}^{2+}]^a$	$[\text{Mg}^{2+}]^a$	$[\text{SO}_4^{2-}]^a$	$f/f_m^b$	CCD <sup>b</sup>	SST <sup>b</sup>	SSS <sup>b</sup>
mmol kg <sup>-1</sup>	mmol kg <sup>-1</sup>	mmol kg <sup>-1</sup>	–	m	°C	–
5	8	5	0.2	500	2.5	1.5

<sup>a</sup>Independent of age; <sup>b</sup>Maximum error at 100 Ma.

#### 461 5.3.4 Summary: Error propagation

462 Despite relatively large assumed parameter errors, the propagated uncertainties in  
 463 our results are moderate, suggesting that our reconstruction method is robust. However,  
 464 the degree of accuracy to which our results reflect reality most critically depends on the  
 465 reconstructed major ion composition of seawater, particularly  $[\text{Ca}^{2+}]$ , for which we have  
 466 to rely on literature values (Fig. 1).

#### 467 5.4 Paleo- $p\text{H}$ scale

468 Proper  $p\text{H}$  scales commonly used for modern seawater are the total scale and  
 469 the seawater scale, which include  $[\text{HSO}_4^-]$  (Eq. (B7)) and  $[\text{HSO}_4^-]+[\text{HF}]$  in their ionic  
 470 medium standard state, respectively (e.g., [Hansson, 1973](#); [Dickson, 1990](#); [Millero,](#)  
 471 [1995](#); [Zeebe and Wolf-Gladrow, 2001](#)). We will focus here on the total scale as the  
 472 concentration of fluoride in seawater is small and essentially unknown in the past. The  
 473 fact that  $[\text{SO}_4^{2-}]$  was lower in the past (Fig. 1a) represents a conceptual and practical  
 474 problem when comparing paleo- $p\text{H}$  and modern ocean  $p\text{H}$ . For instance, envision  
 475 two hypothetical seawater samples of modern and, e.g., Paleocene age with otherwise  
 476 identical composition but different sulfate concentrations, say modern and half of  
 477 modern  $[\text{SO}_4^{2-}]$ . The two samples would give a different  $p\text{H}$  reading relative to a modern  
 478 reference standard due to differences in  $[\text{SO}_4^{2-}]$ . The utility of the total  $p\text{H}$  scale in  
 479 modern seawater implicitly relies on the constancy of the major components: “Sea water  
 480 is an ionic medium [...] with practically constant composition of the major constituents”  
 481 ([Hansson, 1973](#)); “The total concentrations of conservative constituents, such as borate,  
 482 sulfate, and fluoride, can be estimated from salinity” ([Dickson et al., 2007](#)). None of the  
 483 above, of course, holds for paleo-seawater over time scales of millions of years. Hence  
 484 labeling reconstructed  $p\text{H}$  values “ $p\text{H}_T$ ” (e.g., derived from Cenozoic  $\delta^{11}\text{B}$ ), where the  
 485 subscript  $T$  refers to the modern concept of the total  $p\text{H}$  scale makes little sense in light

486 of sulfate changes and should be avoided.

487 To illustrate the effect of  $[\text{SO}_4^{2-}]$  on  $[\text{H}^+]$ , consider Eq. (B7) and Fig. B.3. The ratio  
 488 of free to total hydrogen ion concentration may be estimated from:

$$[\text{H}^+]_F/[\text{H}^+]_T \simeq 1/(1 + [\text{SO}_4^{2-}]/0.1) . \quad (11)$$

489 For further illustration, assume  $[\text{H}^+]_T$  to be constant. Then at half of modern  $[\text{SO}_4^{2-}]$ ,  
 490 Eq. (11) would give a  $\sim 12\%$  higher free hydrogen ion concentration, or a  $\sim 0.05$  units lower  
 491  $p\text{H}_F$ , relative to modern  $[\text{SO}_4^{2-}]$ . While this example is oversimplified compared to actual  
 492 past seawater changes, it illustrates the effect of  $[\text{SO}_4^{2-}]$  on  $p\text{H}$ , which, in turn affects  
 493 speciation, including the  $[\text{B}(\text{OH})_3]/[\text{B}(\text{OH})_4^-]$  fraction, a primary control on their  $^{11}\text{B}/^{10}\text{B}$   
 494 ratio, which is critical for the  $p\text{H}$  proxy. As a result, changes in  $[\text{SO}_4^{2-}]$  by themselves  
 495 would affect  $p\text{H}$  reconstructions, even if all other conditions were the same. The bottom  
 496 line is that the change in past  $[\text{SO}_4^{2-}]$  (Fig. 1a) represents a conceptual and practical  
 497 problem for determining paleo-seawater  $p\text{H}$ . The issue should be worked out properly  
 498 for, e.g.,  $\delta^{11}\text{B}$ -derived  $p\text{H}$  but is beyond the scope of this paper.

## 499 6 Conclusions

500 In this study, we have presented new reconstructions of past ocean carbonate  
 501 chemistry and atmospheric  $\text{CO}_2$  based on recent data and revised calculations. We also  
 502 provide simple corrections for past equilibrium constants, supported by experimental  
 503 data and well-suited for numerical models and observational studies on multi-million  
 504 year time scales. Our updated result for just the seawater carbonate ion concentration  
 505 ( $\sim 2.3$  to 4-fold lower 100 Myr ago) is similar to our earlier work (Tyrrell and Zeebe,  
 506 2004). This holds despite higher  $[\text{Ca}^{2+}]$  from fluid inclusions  $>50$  Ma (compared  
 507 to TZO4), new chemistry routines, incorporation of  $[\text{SO}_4^{2-}]$  effects, alternative CCD  
 508 records, and extensive parameter variations, which suggests that our core approach  
 509 is robust. However, all revised reconstructions using new alkenone and boron data

510 now suggest similar to modern long-term ocean inventories of DIC and TA over the  
511 Cenozoic. This result contrasts with one of our earlier scenarios, which featured high  
512 Paleocene-Eocene DIC/TA inventories and was based on a now outdated boron record.  
513 Overall, our estimated long-term trends in CO<sub>2</sub> system parameters across the Cenozoic  
514 appear consistent, regardless of whether we combine our carbonate ion concentration  
515 with alkenone-derived  $p\text{CO}_2$  or boron-derived  $p\text{H}$ . Our error analysis shows that despite  
516 relatively large assumed parameter errors, the propagated uncertainties in our results  
517 are moderate, lending confidence to our reconstruction method. However, the degree of  
518 accuracy to which our results reflect reality depends primarily on the fidelity of proxies  
519 for past major ion concentrations in seawater, particularly  $[\text{Ca}^{2+}]$ , which is independent  
520 of our work (Fig. 1). Finally, we have identified changes in past seawater sulfate as a  
521 conceptual and practical problem for determining paleo-seawater  $p\text{H}$ , which should be  
522 sorted out properly for the boron-pH proxy.

523 **Acknowledgments.** We thank Lee Kump and one anonymous reviewer for their constructive  
524 comments, which improved the paper. We are grateful to Dr. James William Buchanan Rae for  
525 sharing data compilations. Discussions with Gavin Foster, Sindia Sosdian, Yige Zhang, David  
526 Evans, Laura Haynes, and within the Research Coordination Network on Cenozoic  $p\text{CO}_2$  (NSF  
527 OCE16-36005, Bärbel Hönlisch) provided valuable details on proxy data. This research was  
528 supported by a NSF subaward of OCE13-38842 and NSF award OCE15-58699 to R.E.Z.

529 **Electronic Annex.** Our results displayed in Figs. 5,6 are electronically available at  
530 [www.soest.hawaii.edu/oceanography/faculty/zeebe\\_files/ZT19.html](http://www.soest.hawaii.edu/oceanography/faculty/zeebe_files/ZT19.html).

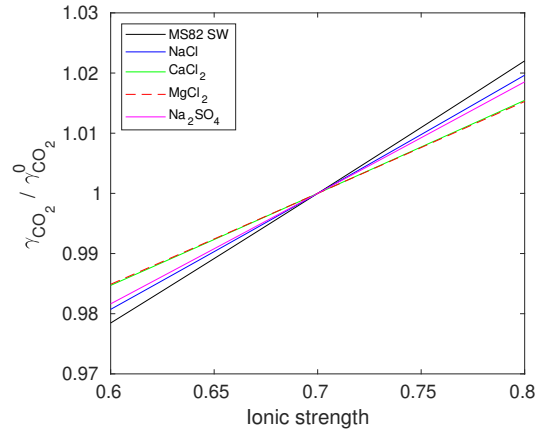


**Figure A.1.** CO<sub>2</sub> activity coefficient ratio for  $\gamma_{CO_2}^0 = \gamma_{CO_2}(I = 0.7)$ . Black line (MS82 SW): seawater (Millero and Schreiber, 1982). Parameters for other components are from He and Morse (1993).

## 531 Appendix A: $a_{H_2O}$ and $\gamma_{CO_2}$

532 Changes in the activity of water ( $a_{H_2O}$ ) and the activity coefficient of dissolved CO<sub>2</sub> ( $\gamma_{CO_2}$ )  
 533 for solution compositions as reconstructed here are small. Moreover, for our approach only  $K^*$   
 534 ratios (past/modern) matter, hence the effect on the  $K_1^*$  ratio (see Eqs. (7) and (10)) is minor.  
 535 The activity of water in seawater was estimated as a function of ionic strength, or salinity  $S$   
 536 (Millero and Leung, 1976; Lund et al., 2003):

$$a_{H_2O} = 1 - 5.0901 \times 10^{-4} S - 6.9567 \times 10^{-7} S^2 . \quad (A1)$$

537 For example, a salinity change from 35 to 33 ( $I$  from 0.72 to 0.68) would give a  $a_{H_2O}$  ratio of  
 538 1.001.

539 The CO<sub>2</sub> activity coefficient ( $\gamma_{CO_2}$ ) for solutions of various seawater salts may be described by:

$$\log \gamma_{CO_2} = k I , \quad (A2)$$

540 where  $k > 0$  (so-called salting out) depends on the type of salt. For the major seawater  
 541 components, variations in  $k$  are moderate and have a minor effect on the ratio  $\gamma_{CO_2} / \gamma_{CO_2}^0$  for  
 542  $\gamma_{CO_2}^0 = \gamma_{CO_2}(I = 0.7)$  (Fig. A.1). Hence we used Eq. (A2) and adopted  $k = 0.0946$  from the  
 543 original IPM to calculate  $\gamma_{CO_2}$  (Millero and Schreiber, 1982).

## 544 Appendix B: [Ca<sup>2+</sup>], [Mg<sup>2+</sup>], [SO<sub>4</sub><sup>2-</sup>] Effects on $K^*$ s: Data

### 545 B.1 [Ca<sup>2+</sup>]

546 Calcium ions in seawater directly interact with major ions such as sulfate, as well as the  
 547 dissolved carbonate species, including HCO<sub>3</sub><sup>-</sup> and CO<sub>3</sub><sup>2-</sup>. Hence changes in the seawater calcium

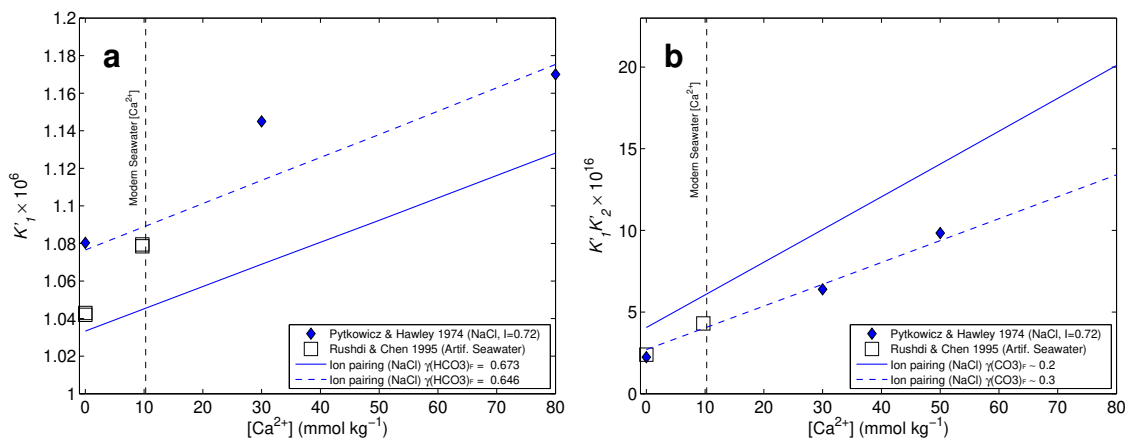


**Figure B.1.** Measured (symbols) changes in (a) apparent  $K_1'$  and (b)  $K_1'K_2'$  as a function of  $[Ca^{2+}]$  in NaCl solutions and artificial seawater (ASW) both at constant ionic strength via adjusting  $[NaCl]$  at  $25^\circ C$  (Pytkowicz and Hawley, 1974; Rushdi and Chen-Tung, 1995). Lines were calculated for PH74's NaCl solutions using their  $k$ ,  $\gamma_{CO_2}$ , and  $a_{H_2O}$ , and an ion-pairing model based on Millero and Schreiber (1982). Note that changing  $\gamma_{CO_3^{2-}}^F$  from 0.2 to 0.3 has virtually no effect on our final results (see Section 5.3).

548 concentration affect the activity of these ions and therefore the stoichiometric equilibrium  
 549 constants. For example, with rising  $[Ca^{2+}]$ , the concentration of, e.g.,  $CaHCO_3^+$  rises, reducing  
 550  $\gamma_{HCO_3^-}$ . As a result,  $K_1^*$  should increase with  $[Ca^{2+}]$  (see Eq. (7)). Importantly, this  $K_1^*-[Ca^{2+}]$   
 551 relationship is confirmed by actual data (Fig. B.1) and is independent of any assumptions about  
 552 activity coefficients (Eq. (7)), or the stability of  $CaHCO_3^+$ , or any other assumptions about ionic  
 553 interactions.

554 Pytkowicz and Hawley (1974) and Rushdi and Chen-Tung (1995) (PH74 and RC95 for short)  
 555 determined changes in apparent dissociation constants such as  $K_1'$  (Fig. B.1):

$$K_1' = \frac{a_H [HCO_3^-]}{[CO_2]}, \quad (B3)$$

556 where  $a_H$  is the hydrogen ion activity defined in the NBS buffer scale (Mehrbach et al., 1973).

557 Substituting activity coefficients as above and using  $a_H = k\{H^+\}$ , yields:

$$K_1' = K_1 k \frac{\gamma_{CO_2}}{\gamma_{HCO_3^-}} a_{H_2O}, \quad (B4)$$

558 where  $k$  is a correction resulting from  $pH$  measurements in concentrated solutions (Hawley and  
 559 Pytkowicz, 1973). Eq. (B4) is equivalent to PH74's Eq. (1) and shows that ratios of  $K_1'$ , say at  
 560 different  $[Ca^{2+}]$ , do not depend on  $\gamma_{H^+}$ , whereas ratios of  $K_1^*$  do (see Eq. (7)). If the solution is  
 561 sulfate- and fluoride-free (as in PH74),  $\gamma_{H^+}$  should be essentially constant (see also Section B.3)  
 562 and hence ratios of  $K_1'$  and  $K_1^*$  should be the same (cf. Eqs. (B4) and (7)). However, RC95's  
 563 artificial seawater (ASW) contained sulfate and fluoride (Kester et al., 1967). Thus, an increase

564 in their ASW  $[\text{Ca}^{2+}]$  would slightly lower free  $[\text{SO}_4^{2-}]$  via  $\text{Ca}^{2+}\text{-SO}_4^{2-}$  interactions and hence  
 565 increase free  $[\text{H}^+]$  and  $\gamma_{\text{H}^+}$  (see Section B.3). As a result, the increase in  $K_1^*$  with  $[\text{Ca}^{2+}]$  in ASW  
 566 should be smaller than shown in Fig. B.1, which shows RC95's reported changes in apparent  $K_1'$ .

567 PH74 and RC95 experimentally determined  $K_1'$  and  $K_1'K_2' = k^2K_1K_2\gamma_{\text{CO}_2}/\gamma_{\text{CO}_3^{2-}}$ , which  
 568 both increase with  $[\text{Ca}^{2+}]$  (Fig. B.1). The experimental trends are roughly captured by MS82's  
 569 ion pairing model (IPM, see note Section 3.1 though). However, with standard parameters, the  
 570 IPM underestimates  $K_1'$  and overestimates absolute  $K_1'K_2'$  values. This is not critical because our  
 571  $K^*$  corrections (see below) are based on trends, not absolute values. Nevertheless, one could  
 572 attempt to reduce the data-model mismatch by changing model parameters such as the model's  
 573 free activity coefficient of  $\text{HCO}_3^-$  ( $\gamma_{\text{HCO}_3^-}^F$ ) in NaCl solutions from  $\sim 0.67$  to  $\sim 0.65$  and  $\text{CO}_3^{2-}$   
 574 ( $\gamma_{\text{CO}_3^{2-}}^F$ ) from 0.2 to 0.3 (Fig. B.1). However, such changes in, e.g.,  $\gamma_{\text{CO}_3^{2-}}^F$  have virtually no effect  
 575 on our final results (see Section 5.3).

576 While we do not recommend such parameter changes (for one, the IPM was designed for  
 577 full seawater, not simplified solutions such as in PH74), one can ask if the  $\gamma_{\text{CO}_3^{2-}}^F$  value of 0.3, for  
 578 instance, would be within a range of values obtained from PH74's analysis. From PH74's data one  
 579 may estimate  $\gamma_{\text{CO}_3^{2-}}^F$  from  $\gamma_{\text{CO}_3^{2-}}^F = k^2 K_1 K_2 / K_1'' K_2''$ , where  $k = 1.134$  and  $K_1'' K_2'' = 0.4866 \times 10^{-16}$   
 580 were both determined experimentally (Hawley and Pytkowicz, 1973; Hawley, 1973). Using values  
 581 for  $K_1$  and  $K_2$  at 25°C (Harned and Davis, 1943; Harned and Scholes, 1941), gives  $\gamma_{\text{CO}_3^{2-}}^F \approx 0.55$   
 582 in NaCl solutions at  $I = 0.72$ . This is significantly higher than estimates for  $\gamma_{\text{CO}_3^{2-}}^F$  in seawater  
 583 at similar ionic strength and points to some inconsistency in PH74's data and/or analysis. One  
 584 possibility (speculation) is that PH74's analysis underestimated  $K_1'' K_2''$  and overestimated the  
 585 stoichiometric association constant of  $\text{NaCO}_3^-$  (Butler and Huston, 1970; Millero and Schreiber,  
 586 1982; Millero and Thurmond, 1983). The above merely illustrates some of the uncertainties  
 587 involved in both models and data of even seemingly simple NaCl- $\text{Ca}^{2+}$ - $\text{HCO}_3^-$  solutions. Note  
 588 that seawater solutions are substantially more complex and that changing parameters to fit one  
 589 particular data set may cause inconsistencies with another (e.g., for  $\gamma_{\text{CO}_3^{2-}}$ , see Section B.4).

## 590 B.2 $[\text{Mg}^{2+}]$

591 Similar to  $\text{Ca}^{2+}$ ,  $\text{Mg}^{2+}$  interacts with various ions in seawater, including  $\text{HCO}_3^-$  and  $\text{CO}_3^{2-}$   
 592 and reduces their activity, which should increase stoichiometric (or apparent) constants with  
 593 rising  $[\text{Mg}^{2+}]$  (see Eqs. (7)-9)). This behavior is confirmed by experimental studies in both  
 594 NaCl solutions and ASW (Fig. B.2). The steeper slope indicated by Millero and Thurmond  
 595 (1983)'s data ( $K^*$ 's) is likely due to the varying ionic strength of their Na-Mg-Cl solutions, which  
 596 increased along with  $[\text{Mg}^{2+}]$  ( $I = [0.56 \text{ } 1.11]$ ). Again, the IPM (Millero and Schreiber, 1982)



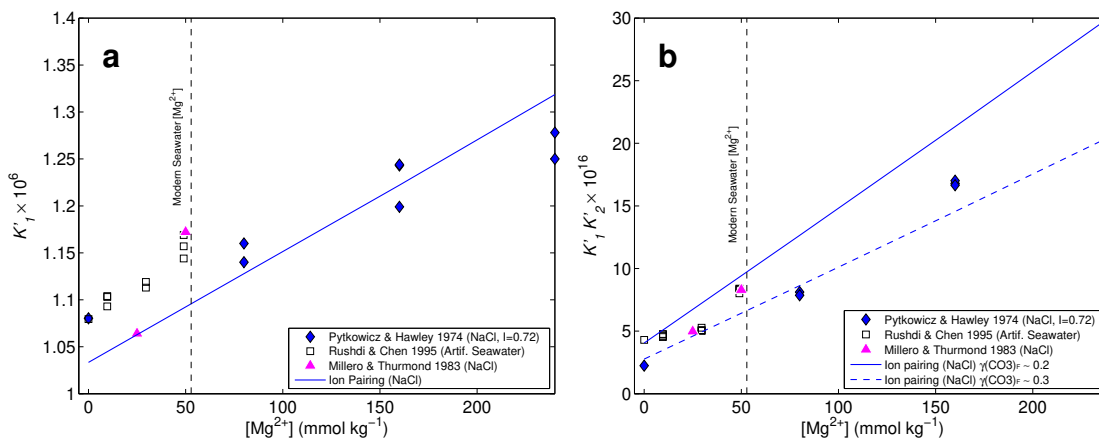


**Figure B.2.:** Measured (symbols) changes in (a) apparent  $K'_1$  and (b)  $K'_1 K'_2$  as a function of  $[\text{Mg}^{2+}]$  in NaCl solutions and artificial seawater (ASW) both at constant ionic strength via adjusting  $[\text{NaCl}]$  at  $25^\circ\text{C}$  (Pytkowicz and Hawley, 1974; Rushdi and Chen-Tung, 1995). The ionic strength of Millero and Thurmond (1983)'s Na-Mg-Cl solutions (triangles) increased along with  $[\text{Mg}^{2+}]$ ,  $I = [0.56 \text{ } 1.11]$  (higher  $I$ 's not shown). Lines were calculated for PH74's NaCl solutions using an ion-pairing model based on Millero and Schreiber (1982). Note that Pytkowicz and Hawley (1974)'s and Rushdi and Chen-Tung (1995)'s data shown are for NaCl solutions without  $\text{Ca}^{2+}$  and ASW with  $\text{Ca}^{2+}$  ( $\sim 9.7 \text{ mmol kg}^{-1}$ ), respectively. Note that changing  $\gamma_{\text{CO}_3}^F$  from 0.2 to 0.3 has virtually no effect on our final results (see Section 5.3).

597 reproduces the values and trend for  $K'_1$  reasonably well but overestimates  $K'_1 K'_2$  (see discussion  
 598 above). Importantly, the details of Mg-effects on dissociation constants for concentrations higher  
 599 than modern ( $[\text{Mg}^{2+}] > 53 \text{ mmol kg}^{-1}$ ) are not critical for the present study because seawater  
 600  $[\text{Mg}^{2+}]$  was likely lower than modern during much of the last 100 Myr (see Section 2).

601 Relevant data on  $K_1^*$  and  $K_2^*$  were also provided by He and Morse (1993). Unfortunately,  
 602 measurements including changes in  $[\text{Ca}^{2+}]$ ,  $[\text{Mg}^{2+}]$ , and  $[\text{SO}_4^{2-}]$  were conducted at different  
 603  $I$ 's and at 0, 50, 75, and  $90^\circ\text{C}$  but not at  $25^\circ\text{C}$ . In addition, possible interpolation to  $25^\circ\text{C}$  is  
 604 hindered by the fact that some of the data appear inconsistent. For example, the value for  $pK_1^*$   
 605 at  $m_{\text{SO}_4^{2-}} = 1 \text{ mmol kg}^{-1}$  and  $50^\circ\text{C}$  seems significantly too low compared to other temperatures  
 606 (see their Table 2).

### 607 B.3 $[\text{SO}_4^{2-}]$

608 In seawater,  $\text{SO}_4^{2-}$  interacts with  $\text{Mg}^{2+}$ ,  $\text{Ca}^{2+}$ ,  $\text{Na}^+$ , etc. In addition, a significant fraction of  
 609 hydrogen ion is bound to sulfate in the form of bisulfate ion:



610 with dissociation constant

$$K'_{\text{HSO}_4^-} = \frac{[\text{H}^+]_F [\text{SO}_4^{2-}]}{[\text{HSO}_4^-]}. \quad (\text{B6})$$

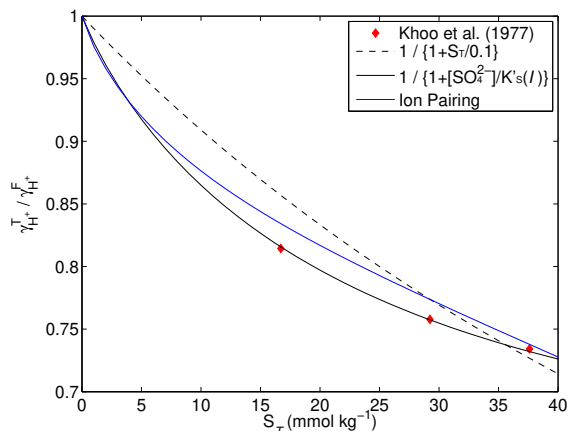


**Figure B.3.**: Effect of total sulfate on the ratio of hydrogen ion activity coefficients  $\gamma_{H^+}^T / \gamma_{H^+}^F = [H^+]_F / [H^+]_T$  at 25°C. Diamonds: based on [Khoo et al. \(1977\)](#)'s Eq. (3), data in their Tables I and IV ( $[HCl] = 0.01 \text{ mol kg}^{-1}$ ), and Eq. (B8). Dashed black line:  $[H^+]_F / [H^+]_T$  from Eq. (B7) using  $S_T$  and a constant  $K'_{\text{HSO}_4^-} = 0.1$  taken from [Dickson \(1990\)](#) ( $T_c = 25^\circ\text{C}$ ,  $S = 35$ ). Solid black line:  $1 / (1 + [\text{SO}_4^{2-}] / K'_{\text{HSO}_4^-})$  using  $[\text{SO}_4^{2-}]$  and [Khoo et al. \(1977\)](#)'s  $K'_{\text{HSO}_4^-}$ , including its variation with ionic strength  $I$ . Blue line: ion-pairing model ([Miller and Schreiber, 1982](#)) using [Khoo et al. \(1977\)](#)'s solution compositions,  $K'_{\text{HSO}_4^-}$ , and their effective (real) ionic strength.

611 Note that  $K'_{\text{HSO}_4^-}$  is given in terms of the free (not total) hydrogen ion concentration; hence the  
 612 prime instead of an asterisk. Thus, changes in total seawater sulfate,  $S_T = [\text{SO}_4^{2-}] + [\text{HSO}_4^-]$ ,  
 613 cause changes in the free concentration of hydrogen ions. In fact, the bisulfate dissociation in  
 614 seawater (Eq. (B5)) represents the very basis for the total  $p\text{H}$  scale in seawater, where the total  
 615 hydrogen ion concentration is given by (e.g., [Hansson, 1973](#); [Dickson, 1990](#)):

$$[\text{H}^+]_T = [\text{H}^+]_F + [\text{HSO}_4^-] = [\text{H}^+]_F (1 + S_T / K'_{\text{HSO}_4^-}) . \quad (\text{B7})$$

616 The effect of sulfate on, e.g.,  $K_1^*$  and  $K_2^*$  may be illustrated by means of Eqs. (7) and (8). Assume  
 617 for the moment that the activities of  $\text{CO}_2$ ,  $\text{HCO}_3^-$ , and  $\text{CO}_3^{2-}$  remain constant. Then an increase  
 618 in  $S_T$  would reduce  $[\text{H}^+]_F$  (Eq. (B5)) and hence  $\gamma_{\text{H}^+}$ . As a result,  $K_1^*$  and  $K_2^*$  would increase with  
 619 the total sulfate concentration in seawater (Eqs. (7) and (8)). It turns out that changes in sulfate  
 620 have a minor effect on the overall activities of  $\text{CO}_2$ ,  $\text{HCO}_3^-$ , and  $\text{CO}_3^{2-}$ , which do not directly  
 621 interact with  $\text{SO}_4^{2-}$  (though the direct effect on  $\text{Ca}^{2+}$  and hence calcite solubility is significant,  
 622 see Fig. 3). Thus, given a value for  $K'_{\text{HSO}_4^-}$ , the effect of changing total seawater sulfate on  $K_1^*$   
 623 and  $K_2^*$  may be estimated.

624 Data for  $K'_{\text{HSO}_4^-}$  have been obtained from galvanic cell measurements from which also the  
 625 ratio  $\gamma_{\text{H}^+}^T / \gamma_{\text{H}^+}^F$  as a function of  $S_T$  can be calculated (e.g., [Khoo et al., 1977](#); [Dickson, 1990](#))  
 626 (Fig. B.3). For example, [Khoo et al. \(1977\)](#) determined HCl activity coefficients in ASW with and  
 627 without sulfate. Rearranging their Eq. (3) yields an expression for the mean activity coefficient

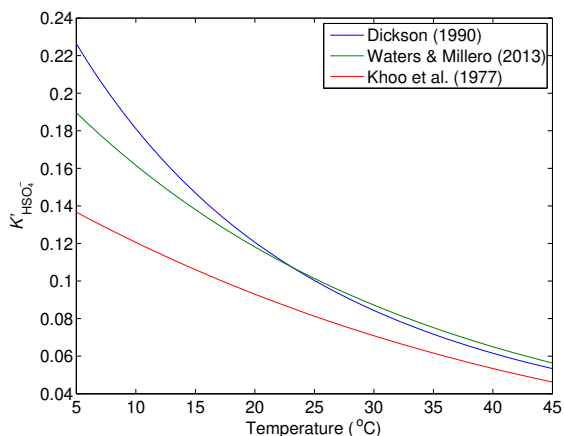


**Figure B.4.:** Values for  $K'_{\text{HSO}_4^-}$ , the dissociation constant of bisulfate in seawater as a function of temperature ( $S = 35$ ) provided by different studies (Dickson, 1990; Waters and Millero, 2013; Waters et al., 2014; Khoo et al., 1977).

628 of HCl,  $\gamma_{\pm}(\text{HCl})$ , which can be evaluated using the data given in their Tables I and IV. The ratio  
 629  $\gamma_{\text{H}^+}^T/\gamma_{\text{H}^+}^F$  at different  $S_T$  may then be estimated using the rule  $\gamma_{\pm} = (\gamma_+ \gamma_-)^{1/2}$  (Robinson and  
 630 Stokes, 1959):

$$\gamma_{\text{H}^+}^T/\gamma_{\text{H}^+}^F = \gamma_{\pm}^2(\text{HCl})/\gamma_{\pm}^2(\text{HCl}) \quad (\text{B8})$$

631 where primed and unprimed  $\gamma$ 's refer to a given  $S_T$  and  $S_T = 0$  (ASW with and without  $\text{SO}_4^{2-}$ ),  
 632 respectively. Note that  $\text{SO}_4^{2-}$  effects on  $\gamma_{\text{Cl}^-}$  should be small and hence  $\gamma_{\text{Cl}^-}$  and  $\gamma'_{\text{Cl}^-}$  cancel.

633 For Khoo et al. (1977)'s experimental conditions, Eq. (B8) indicates a  $\sim 25\%$  drop in  
 634  $\gamma_{\text{H}^+}^T/\gamma_{\text{H}^+}^F = [\text{H}^+]_F/[\text{H}^+]_T$  as  $S_T$  rises from 0  $\text{mmol kg}^{-1}$  to seawater values of  $\sim 28 \text{ mmol kg}^{-1}$  ( $S_T$   
 635 scaled linearly with salinity  $S$ ) (Fig. B.3). A similar trend is obtained for  $[\text{H}^+]_F/[\text{H}^+]_T$  ratios  
 636 estimated from Eq. (B7) with a constant  $K'_{\text{HSO}_4^-} = 0.1$  taken from Dickson (1990) (Fig. B.3). The  
 637 latter graph is shown merely to visualize Eq. (B7), which uses  $S_T$  and is plotted for constant  
 638  $K'_{\text{HSO}_4^-}$ . Eq. (B7) is not supposed to fit Khoo et al. (1977)'s data which were obtained at low  $\text{pH}$   
 639 (requiring consideration of  $[\text{SO}_4^{2-}]$  instead of  $S_T$ ) and varying salinity/ionic strength ( $I$ ). Rather,  
 640 the data should fit the expression  $[\text{H}^+]_F = [\text{H}^+]_T/(1 + [\text{SO}_4^{2-}]/K'_{\text{HSO}_4^-})$ , where  $K'_{\text{HSO}_4^-}$  varies with  
 641  $I$ . Using  $K'_{\text{HSO}_4^-}$  from Khoo et al. (1977), this is indeed the case (Fig. B.3) and is unsurprising  
 642 because  $K'_{\text{HSO}_4^-}$  was actually derived by a data fit of a similar kind (Khoo et al., 1977). In  
 643 summary, the free hydrogen ion concentration decreases, and hence  $K_1^*$  and  $K_2^*$  increase, with  
 644 the total sulfate concentration in seawater (Eqs. (7) and (8)).

645 The magnitude of the predicted change in  $K_1^*$  and  $K_2^*$  with sulfate depends on  $K'_{\text{HSO}_4^-}$  in  
 646 seawater, which is challenging to determine analytically. At  $T_c = 25^\circ\text{C}$  and  $S = 35$ , Dickson  
 647 (1990)'s value is  $\sim 20\%$  higher than that given by Khoo et al. (1977) (Fig. B.4). In his approach,

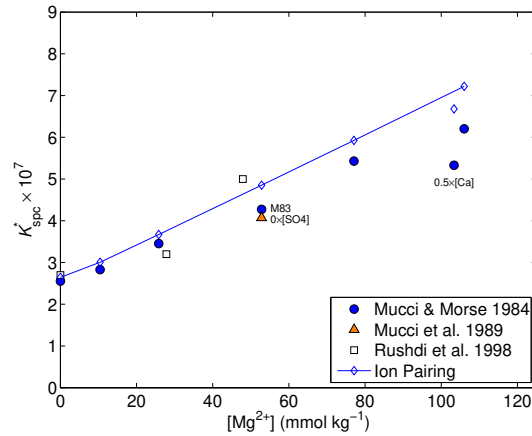


**Figure B.5.:** Changes in  $K'_{\text{spc}}$  as a function of  $[\text{Mg}^{2+}]$  from experiments in ASW at constant ionic strength via adjusting  $[\text{NaCl}]$  at  $25^\circ\text{C}$  (symbols); M83 = Mucci (1983). Data points labeled 0.5 $\times$ [Ca] and 0 $\times$ [SO<sub>4</sub>] refer to ASW at half seawater-[Ca<sup>2+</sup>] and sulfate-free ASW (Mucci et al., 1989). The open diamonds were calculated for Mucci and Morse's (1984) ASW solutions using an ion-pairing model based on Millero and Schreiber (1982).

648 Dickson included estimates of changes in  $\gamma_{\text{H}^+}$  with  $[\text{HCl}]$ ; Khoo et al. (1977) did not. Furthermore,  
 649 Dickson's values  $>25^\circ\text{C}$  are in close agreement with values based on a recent re-evaluation of  
 650 existing data for  $K'_{\text{HSO}_4^-}$  (Waters and Millero, 2013; Waters et al., 2014). Hence, in this study we  
 651 use  $K'_{\text{HSO}_4^-} = 0.1$  at  $T_c = 25^\circ\text{C}$  and  $S = 35$  (Dickson, 1990). Importantly, this implies a weaker  
 652 association constant  $\beta_{\text{HSO}_4^-} = 1/K'_{\text{HSO}_4^-}$  for  $\text{HSO}_4^-$  (see Eq. (B6)) than suggested by Khoo et al.  
 653 (1977).

#### 654 B.4 Calcite solubility

655 It appears that few experimental studies have systematically examined the effect of  $[\text{Mg}^{2+}]$   
 656 and  $[\text{Ca}^{2+}]$  on the solubility product of calcite,  $K'_{\text{spc}}$  (Eq. (6)). Mucci and Morse (1984) varied  
 657  $[\text{Mg}^{2+}]$  in ASW up to about double the modern value at constant  $I$  (Fig. B.5). Calcium was  
 658 kept close to modern values at  $\sim 10\text{--}12$   $\text{mmol kg}^{-1}$  except for one run with half of modern  $[\text{Ca}^{2+}]$   
 659 (labeled 0.5 $\times$ [Ca]). As expected from  $\text{Mg}^{2+}\text{-CO}_3^{2-}$  interactions and Eq. (9),  $K'_{\text{spc}}$  increases with  
 660  $[\text{Mg}^{2+}]$ . A comparable trend was found by Rushdi et al. (1998) in similar manipulations of  
 661 ASW (Fig. B.5). The IPM (Millero and Schreiber, 1982) overestimates  $K'_{\text{spc}}$  at higher  $[\text{Mg}^{2+}]$  by  
 662  $\sim 10\text{--}20\%$ . Note that if this mismatch was entirely attributed to model  $\gamma_{\text{CO}_3^{2-}}$ , then the inferred  
 663 error would be much smaller than the inferred error in  $\gamma_{\text{CO}_3^{2-}}$  based on  $K'_1K'_2$  (discussed above).

664 Regarding uncertainties in the experimental results, it is important that both  $[\text{Ca}^{2+}]$  and  
 665  $[\text{CO}_3^{2-}]$  are required to determine  $K'_{\text{spc}}$ . While Mucci and Morse (1984) measured  $[\text{Ca}^{2+}]$  directly  
 666 by titration,  $[\text{CO}_3^{2-}]$  was derived from carbonate alkalinity,  $p\text{H}$ , and  $K'_2$ , where  $K'_2$  was actually

667 estimated based on ion pairing equations of [Millero and Schreiber \(1982\)](#). [Rushdi et al. \(1998\)](#)  
 668 also involved  $K'_2$  to calculate  $[\text{CO}_3^{2-}]$  but it is not obvious from their description what values they  
 669 used for  $K'_2$ . The  $K_{\text{spc}}^*$  values of those studies are thus not ‘true’ experimental values because  
 670 they partly rely on theoretical estimates of  $K'_2$  in ASW of varying compositions to derive  $[\text{CO}_3^{2-}]$ .  
 671 Hence, in addition to measurement uncertainties, the  $K_{\text{spc}}^*$  values from experiments in ASW  
 672 shown in Fig. B.5 are also subject to errors in  $K'_2$  and  $[\text{CO}_3^{2-}]$  estimates.

673 Additional calcite solubility studies are available in the literature, including [He and Morse](#)  
 674 [\(1993\)](#) who stated that calcite solubility in three synthetic brines was measured and referred  
 675 to  $m_{\text{CO}_3^{2-}}$  as analytical data but no details were given and no values for  $K_{\text{spc}}^*$  and  $m_{\text{CO}_3^{2-}}$  were  
 676 listed. [Gledhill and Morse \(2006\)](#) reported calcite solubility in Na-Ca-Mg-Cl brines up to  $I \approx 4.5$ .  
 677 However,  $I$  varied substantially, the carbonate ion concentration was calculated using a Pitzer  
 678 model, and most low- $I$  data had very similar  $\text{Mg}^{2+}$  and  $\text{Ca}^{2+}$  concentrations, which is unhelpful  
 679 for the current problem. [Wolf et al. \(1989\)](#) studied calcite solubility in different electrolytes,  
 680 yet only Pitzer-calculated  $K_{\text{spc}}^*$  values were provided for NaCl solutions. We are not aware of a  
 681 study that systematically varied  $[\text{Ca}^{2+}]$  at constant ionic strength and provided measured values  
 682 for  $K_{\text{spc}}^*$ . Note that  $\text{Ca}^{2+}$  directly affects  $K_{\text{spc}}^*$  through its activity coefficient (see Eq. (9)) and  
 683 indirectly via interactions with  $\text{CO}_3^{2-}$ .

684 [Mucci et al. \(1989\)](#) provided a  $K_{\text{spc}}^*$  value for sulfate-free ASW (labeled  $0 \times [\text{SO}_4]$ , Fig. B.5).  
 685 However, experiments were only conducted at  $25^\circ\text{C}$  and  $K'_2$  was again estimated based on an  
 686 ion pairing model. Several industrial/engineering studies are also available on calcite solubility  
 687 in mixed electrolytes including  $\text{SO}_4^{2-}$  (e.g., [Chong and Sheikholeslami, 2001](#); [Shi et al., 2013](#); [Dai](#)  
 688 [et al., 2017](#)). However, these studies calculated  $[\text{CO}_3^{2-}]$  using thermodynamic constants or Pitzer  
 689 equations, were restricted to  $60\text{--}80^\circ\text{C}$  ([Chong and Sheikholeslami, 2001](#)), or to a single high  
 690 NaCl background concentration  $>4$  M ([Shi et al., 2013](#); [Dai et al., 2017](#)).

## 691 Appendix C: $K^*$ Ratios

692 The  $K^*$  ratios calculated with the IPM are very nearly linear as a function of  $[\text{Ca}^{2+}]$ ,  $[\text{Mg}^{2+}]$ ,  
 693 and  $[\text{SO}_4^{2-}]$  ( $x_j$ 's), even when the  $x_j$ 's are varied in combination (illustrated for  $K_1^*$  in Fig. C.1).  
 694 Hence over the relevant  $x_j$  range for reconstructions over the past 100 Myr (Section 2), the full  
 695 IPM results and the linear approximation (Eq. (10)) are essentially indistinguishable (planes are  
 696 nearly flat, Fig. C.1). Differences are only discernible at low  $[\text{SO}_4^{2-}]$ , where two separate planes  
 697 are visible. The root mean square errors of the linear approach for  $K_1^*$ ,  $K_2^*$ , and  $K_{\text{spc}}^*$  relative to  
 698 the IPM results are about 0.5%, 2%, and 1%, much smaller than the accuracy required here. The

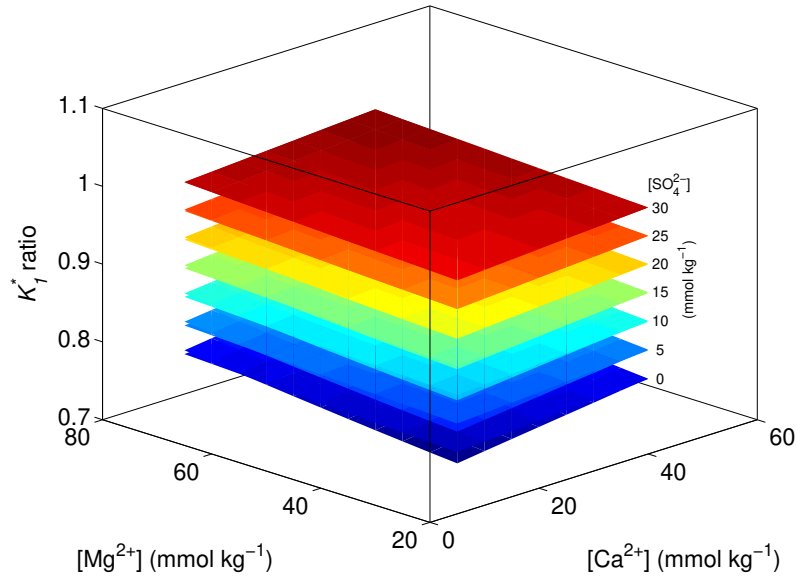


**Figure C.1.:**  $K_1^*$  ratio (relative to modern) calculated with the IPM (Millero and Schreiber, 1982) and the linear approximation (Eq. (10)). The results are virtually indistinguishable, except at low  $[SO_4^{2-}]$ , where two separate planes are barely visible.

699 largest error occurs for  $K_2^*$  at low  $[SO_4^{2-}]$  and both high  $[Ca^{2+}]$  and  $[Mg^{2+}]$  (not shown). However,  
 700 this is of minor importance for the present study because  $[Ca^{2+}]$  and  $[Mg^{2+}]$  are inversely  
 701 correlated over much of the past 100 Myr (Section 2).

## 702 Appendix D: Sensitivity Parameters for $I = \text{const.}$

**Table D1.:** Sensitivity parameters  $s_{ij} \times 10^3$  (dimensionless) for Eq. (10) at constant ionic strength via NaCl adjustment.

	$K_1^*$	$K_2^*$	$K_{\text{spc}}^*$
$Ca^{2+}$	6	156	171
$Mg^{2+}$	22	415	471
$SO_4^{2-}$	203	162	22

## 703 Appendix E: CCD variations and $\Omega$

704 Our surface  $[CO_3^{2-}]$  is calculated from Eq. (1):

$$[CO_3^{2-}] = \Omega \cdot K_{\text{sp}}^* / [Ca^{2+}], \quad (\text{Eg})$$

705 which includes the direct effect of past changes in  $[Ca^{2+}]$ , and  $T$ ,  $S$ ,  $[Ca^{2+}]$ ,  $[Mg^{2+}]$ , and  $[SO_4^{2-}]$   
 706 via  $K_{\text{sp}}^*$  on  $[CO_3^{2-}]$ . In addition, whole/deep-ocean saturation has varied somewhat in the past for

707 which we apply a correction ( $\beta$ ) based on CCD records (Tyrrell and Zeebe, 2004), i.e.,  $\Omega = \beta \Omega_m$   
 708 ( $m =$  modern). Note that  $\Omega$  in the ocean at any  $z$  and at a given time  $t$  and  $[\text{Ca}^{2+}]$  is a function  
 709 of  $[\text{CO}_3^{2-}]$  but not of  $[\text{Ca}^{2+}]$  (homogeneous), because:

$$\Omega = ([\text{CO}_3^{2-}] [\text{Ca}^{2+}]) / ([\text{CO}_3^{2-}]_{\text{sat}} [\text{Ca}^{2+}]_{\text{sat}}) = [\text{CO}_3^{2-}] / [\text{CO}_3^{2-}]_{\text{sat}} . \quad (\text{E10})$$

710 The depth profile of the critical (saturation)  $[\text{CO}_3^{2-}]_{\text{sat}}$ , say modern, is given by:

$$c = a \exp[b(z - z_0)] , \quad (\text{E11})$$

711 where  $a, b, z_0$  are constants (Jansen et al., 2002). The crossover of *in situ* and saturation  $[\text{CO}_3^{2-}]$   
 712 determines the depth of the saturation horizon  $z_{sh}$ . Specifically, consider Eq. (E11) being applied  
 713 twice, once for  $c = c_{sh}$  at  $z_{sh}$  (at an initial  $[\text{CO}_3^{2-}]$ ), and once for  $c = c'_{sh}$  at a new  $z'_{sh}$  and a  
 714 new  $[\text{CO}_3^{2-}]$  (with  $[\text{Ca}^{2+}]$  the same in both). Then  $c'_{sh}/c_{sh}$  provides a ratio relating changes in  
 715 saturation to saturation depth (from Eq. (E11)):

$$c'_{sh}/c_{sh} = \exp[b(z'_{sh} - z_{sh})] . \quad (\text{E12})$$

716 For a given CCD ( $z_{cc}$ ) at time  $t$ , the saturation horizon is  $z_{sh} = z_{cc} - \Delta z$ , hence:

$$c'_{sh}/c_{sh} = \exp[b(z'_{sh} - z_{cc})] , \quad (\text{E13})$$

717 assuming that  $\Delta z$  does not vary with  $[\text{CO}_3^{2-}]$  (all else being equal). Importantly, it is immaterial  
 718 here whether  $\Delta z$  has varied in the past because it cancels out. For past conditions (subscript  $p$ ),  
 719 we can write:

$$(c'_{sh}/c_{sh})_p = \exp[b_p(z'_{sh} - z_{cc})_p] , \quad (\text{E14})$$

720 i.e., the same relationship, except for  $b_p$ , which, however, only varies slightly. Between modern  
 721 and, say, Eocene conditions (including a 10 K temperature rise),  $b$  changes by only  $\sim 13\%$ . Also,  
 722 variations in  $b$  have a small effect on our results. Thus, we correct (scale) our surface  $\Omega$  with the  
 723 corresponding deep ratio based on the CCD record over time ( $z_{cc}(t)$ ) by:

$$\beta = \exp\{b[z_{cc}(t) - z_{cc}(0)]\} \quad (\text{E15})$$

724 and quantify the sensitivity to changes in the surface-to-deep ratio by varying  $f/f_m$  (see  
 725 Section 5.3.3 and Tyrrell and Zeebe (2004)).

## References

- 726 **References**
- 727 Anagnostou, E., E. H. John, K. M. Edgar, G. L. Foster, A. Ridgwell, G. N. Inglis, R. D. Pancost,  
728 D. J. Lunt, and P. N. Pearson (2016). Changing atmospheric CO<sub>2</sub> concentration was the  
729 primary driver of early Cenozoic climate. *Nature* 533, 380–384.
- 730 Bartoli, G., B. Hönisch, and R. E. Zeebe (2011). Atmospheric CO<sub>2</sub> decline during the  
731 Pliocene intensification of Northern Hemisphere glaciations. *Paleoceanogr.* 26, PA4213,  
732 doi:10.1029/2010PA002055.
- 733 Ben-Yaakov, S. and M. B. Goldhaber (1973). The influence of sea water composition on the  
734 apparent constants of the carbonate system. *Deep-Sea Res.* 20, 87–99.
- 735 Berner, E. K. and R. A. Berner (2012). *Global environment: water, air, and geochemical cycles*  
736 (2nd Ed.). Princeton University Press, Princeton, NJ. pp. 444.
- 737 Berner, R. A. (2006). Inclusion of the weathering of volcanic rocks in the GEOCARBSULF  
738 model. *Am. J. Sci.* 306, 295–302.
- 739 Berner, R. A. (2008). Addendum to “Inclusion of the weathering of volcanic rocks in the  
740 GEOCARBSULF model”: (R. A. Berner, 2006, V. 306, p. 295-302). *Am. J. Sci.* 308, 100–103.
- 741 Berner, R. A. and Z. Kothavala (2001). GEOCARB III: A revised model of atmospheric CO<sub>2</sub>  
742 over Phanerozoic time. *Am. J. Sci.* 304, 397–437.
- 743 Boudreau, B. P. and Y. Luo (2017). Retrodiction of secular variations in deep-sea CaCO<sub>3</sub> burial  
744 during the Cenozoic. *Earth Planet. Sci. Lett.* 474, 1–12.
- 745 Brennan, S. T., T. K. Lowenstein, and D. I. Cendon (2013). The major-ion composition of  
746 Cenozoic seawater: The past 36 million years from fluid inclusions in marine halite. *American*  
747 *Journal of Science* 313, 713–775.
- 748 Butler, J. N. and R. Huston (1970). Activity coefficients and ion pairs in the systems sodium  
749 chloride-sodium bicarbonate-water and sodium chloride-sodium carbonate-water. *J. Phys.*  
750 *Chem.* 74(15), 2976–2983.
- 751 Caldeira, K. and R. Berner (1999). Seawater pH and atmospheric carbon dioxide.  
752 *Science* 286(5447), 2043a.
- 753 Chong, T. H. and R. Sheikholeslami (2001). Thermodynamics and kinetics for mixed calcium  
754 carbonate and calcium sulfate precipitation. *Chem. Engineer. Sci.* 56(18), 5391–5400.
- 755 Coggon, R. M., D. A. H. Teagle, C. E. Smith-Duque, J. C. Alt, and M. J. Cooper (2010).  
756 Reconstructing Past Seawater Mg/Ca and Sr/Ca from Mid-Ocean Ridge Flank Calcium  
757 Carbonate Veins. *Science* 327, 1114.
- 758 Dai, Z., A. T. Kan, W. Shi, F. Yan, F. Zhang, N. Bhandari, G. Ruan, Z. Zhang, Y. Liu,  
759 H. A. Alsaiani, Y.-T. Lu, G. Deng, and M. B. Tomson (2017). Calcite and barite solubility  
760 measurements in mixed electrolyte solutions and development of a comprehensive model  
761 for water-mineral-gas equilibrium of the Na-K-Mg-Ca-Ba-Sr-Cl-SO<sub>4</sub>-CO<sub>3</sub>-HCO<sub>3</sub>-CO<sub>2</sub>(aq)-H<sub>2</sub>O  
762 System up to 250°C and 1500 bar. *Industr. Engineer. Chem. Res.* 56(23), 6548–6561.
- 763 Dickson, A. G. (1990). Standard potential of the reaction: AgCl(s) + 1/2 H<sub>2</sub>(g) = Ag(s) +  
764 HCl(aq), and the standard acidity constant of the ion HSO<sub>4</sub><sup>-</sup> in synthetic sea water from  
765 273.15 to 318.15 K. *J. Chem. Thermodyn.* 22, 113–127.
- 766 Dickson, A. G., C. L. Sabine, and J. R. Christian (2007). *Guide to best practices for ocean CO<sub>2</sub>*  
767 *measurements*. PICES Special Publication 3, 191 pp.



- 768 Dickson, J. A. D. (2002). Fossil echinoderms as monitor of the Mg/Ca ratio of Phanerozoic  
769 oceans. *Science* 298, 1222–1224.
- 770 Evans, D. and W. Müller (2012). Deep time foraminifera Mg/Ca paleothermometry: Nonlinear  
771 correction for secular change in seawater Mg/Ca. *Paleoceanography* 27, PA4205.
- 772 Foster, G. L., C. H. Lear, and J. W. B. Rae (2012). The evolution of pCO<sub>2</sub>, ice volume and  
773 climate during the middle Miocene. *Earth Planet. Sci. Lett.* 341, 243–254.
- 774 Garrels, R. M. and M. E. Thompson (1962). A chemical model for seawater at 25°C and one  
775 atmosphere total pressure. *Am. J. Sci.* 260, 57–66.
- 776 Gillis, K. M. and L. A. Coogan (2011). Secular variation in carbon uptake into the ocean crust.  
777 *Earth Planet. Sci. Lett.* 302, 385–392.
- 778 Gledhill, D. K. and J. W. Morse (2006). Calcite solubility in Na-Ca-Mg-Cl brines. *Chem. Geol.* 233,  
779 249–256.
- 780 Gothmann, A. M., J. Stolarski, J. F. Adkins, B. Schoene, K. J. Dennis, D. P. Schrag, M. Mazur,  
781 and M. L. Bender (2015). Fossil corals as an archive of secular variations in seawater chemistry  
782 since the Mesozoic. *Geochim. Cosmochim. Acta* 160, 188–208.
- 783 Hansson, I. (1973). A new set of pH-scales and standard buffers for sea water. *Deep-Sea Res.* 20,  
784 479–491.
- 785 Harned, H. S. and R. Davis (1943). The ionization constant of carbonic acid in water and the  
786 solubility of carbon dioxide in water and aqueous salt solutions from 0 to 50°. *J. Am. Chem.*  
787 *Soc.* 65(10), 2030–2037.
- 788 Harned, H. S. and S. R. Scholes (1941). The ionization constant of HCO<sub>3</sub><sup>-</sup> from 0 to 50°. *J. Am.*  
789 *Chem. Soc.* 63(6), 1706–1709.
- 790 Hauzer, H., D. Evans, W. Müller, Y. Rosenthal, and J. Erez (2018). Calibration of Na partitioning  
791 in the calcitic foraminifer *Operculina ammonoides* under variable Ca concentration: Toward  
792 reconstructing past seawater composition. *Earth Planet. Sci. Lett.* 497, 80–91.
- 793 Hawley, J. E. (1973). *Bicarbonate and carbonate ion association with sodium, magnesium and calcium*  
794 *at 25°C and 0.72 ionic strength*. Ph. D. thesis, Oregon State University.
- 795 Hawley, J. E. and R. M. Pytkowicz (1973). Interpretation of pH measurements in concentrated  
796 electrolyte solutions. *Mar. Chem.* 1(3), 245–250.
- 797 Haynes, L. L., B. Hönisch, K. A. Dyez, K. Holland, Y. Rosenthal, C. R. Fish, A. V. Subhas,  
798 and J. W. B. Rae (2017). Calibration of the B/Ca proxy in the planktic foraminifer *Orbulina*  
799 *universa* to Paleocene seawater conditions. *Paleoceanogr.* 32, 580–599.
- 800 He, S. and J. W. Morse (1993). The carbonic acid system and calcite solubility in aqueous  
801 Na-K-Ca-Mg-Cl-SO<sub>4</sub> solutions from 0 to 90°C. *Geochim. Cosmochim. Acta* 57, 3533–3554.
- 802 Hönisch, B., A. Ridgwell, D. N. Schmidt, E. Thomas, S. J. Gibbs, A. Sluijs, R. Zeebe, L. Kump,  
803 R. C. Martindale, S. E. Greene, W. Kiessling, J. Ries, J. C. Zachos, D. L. Royer, S. Barker,  
804 T. M. Marchitto, R. Moyer, C. Pelejero, P. Ziveri, G. L. Foster, and B. Williams (2012). The  
805 Geological Record of Ocean Acidification. *Science* 335, 1058–1063.
- 806 Horita, J., H. Zimmermann, and H. D. Holland (2002). Chemical evolution of seawater during  
807 the Phanerozoic: Implications from the record of marine evaporites. *Geochim. Cosmochim.*  
808 *Acta* 66(21), 3733–3756.

- 809 Jansen, H., R. E. Zeebe, and D. A. Wolf-Gladrow (2002). Modeling the dissolution of settling  
810  $\text{CaCO}_3$  in the ocean. *Global Biogeochem. Cycles* 16(2), 10.1029/2000GB001279.
- 811 Kester, D. R., I. W. Duedall, D. N. Connors, and R. M. Pytkowicz (1967). Preparation of Artificial  
812 Seawater. *Limnol. and Oceanogr.* 12, 176–179.
- 813 Khoo, K. H., R. W. Ramette, C. H. Culbertson, and R. G. Bates (1977). Determination of  
814 hydrogen ion concentrations in seawater from 5 to 40 °C: standard potentials at salinities from  
815 20 to 45 permil. *Anal. Chem.* 49, 29–34.
- 816 Komar, N., R. E. Zeebe, and G. R. Dickens (2013). Understanding long-term carbon cycle trends:  
817 The late Paleocene through the early Eocene. *Paleoceanogr.* 28, 650–662.
- 818 Kump, L. R., T. J. Bralower, and A. Ridgwell (2009). Ocean Acidification in Deep Time.  
819 *Oceanogr.* 22(4), 94–107.
- 820 Lécuyer, C. (2016). Seawater residence times of some elements of geochemical interest and the  
821 salinity of the oceans. *Bull. Soc. géol. France* 187(6), 245–260.
- 822 Lemarchand, D., J. Gaillardet, É. Lewin, and C. J. Allègre (2002). Boron isotope systematics in  
823 large rivers: implications for the marine boron budget and paleo-pH reconstruction over the  
824 Cenozoic. *Chem. Geol.* 190, 123–140.
- 825 Locklair, R. E. and A. Lerman (2005). A model of Phanerozoic cycles of carbon and calcium  
826 in the global ocean: Evaluation and constraints on ocean chemistry and input fluxes. *Chem.*  
827 *Geol.* 217, 113–126.
- 828 Lowenstein, T. K. (2006). Elevated Eocene atmospheric  $\text{CO}_2$  and its subsequent decline.  
829 *Science* 313, 1928.
- 830 Lowenstein, T. K., L. A. Hardie, and M. N. Timofeeff (2003). Secular variation in seawater  
831 chemistry and the origin of calcium chloride basinal brines. *Geology* 31, 857.
- 832 Lund, M., B. Jönsson, and T. Pedersen (2003). Activity coefficients in sea water using Monte  
833 Carlo simulations. *Mar. Chem.* 80(2-3), 95–101.
- 834 Martínez-Botí, M. A., G. L. Foster, T. B. Chalk, E. J. Rohling, P. F. Sexton, D. J. Lunt, R. D.  
835 Pancost, M. P. S. Badger, and D. N. Schmidt (2015). Plio-Pleistocene climate sensitivity  
836 evaluated using high-resolution  $\text{CO}_2$  records. *Nature* 518, 49–54.
- 837 May, P. M. and D. Rowland (2017). Thermodynamic modeling of aqueous electrolyte systems:  
838 Current status. *J. Chem. Engineer. Data* 62(9), 2481–2495.
- 839 Mehrbach, C., C. H. Culbertson, J. E. Hawley, and R. M. Pytkowicz (1973). Measurement of the  
840 apparent dissociation constant of carbonic acid in seawater at atmospheric pressure. *Limnol.*  
841 *Oceanogr.* 18, 897–907.
- 842 Millero, F. J. (1995). Thermodynamics of the carbon dioxide system in the oceans. *Geochim.*  
843 *Cosmochim. Acta* 59, 661–677.
- 844 Millero, F. J. and W. H. Leung (1976). The thermodynamics of seawater at one atmosphere. *Am.*  
845 *J. Sci.* 276, 1035–1077.
- 846 Millero, F. J. and D. R. Schreiber (1982). Use of the ion pairing model to estimate activity  
847 coefficients of the ionic components of natural waters. *Am. J. Sci.* 282, 1508–1540.
- 848 Millero, F. J. and V. Thurmond (1983). The ionization of carbonic acid in Na-Mg-Cl solutions at  
849 25°C. *J. Sol. Chem.* 12(6), 401–412.

- 850 Montañez, I. P. (2002). Biological skeletal carbonate records changes in major-ion chemistry of  
851 paleo-oceans. *Proc. Nat. Acad. Sci.* 99, 15852–15854.
- 852 Mucci, A. (1983). The solubility of calcite and aragonite in seawater at various salinities,  
853 temperatures, and one atmosphere total pressure. *Am. J. Sci.* 283, 780–799.
- 854 Mucci, A., R. Canuel, and S. Zhong (1989). The solubility of calcite and aragonite in sulfate-free  
855 seawater and seeded growth kinetics and composition of precipitates at 25°C. *Chem. Geol.* 74,  
856 309–329.
- 857 Mucci, A. and J. W. Morse (1984). The solubility of calcite in seawater solutions of various  
858 magnesium concentration,  $I_t = 0.697$  m at 25°C and one atmosphere total pressure. *Geochim.*  
859 *Cosmochim. Acta* 48, 815–822.
- 860 Pagani, M., M. Huber, Z. Liu, S. M. Bohaty, J. Henderiks, W. Sijp, S. Krishnan, and R. M.  
861 DeConto (2011). The Role of Carbon Dioxide During the Onset of Antarctic Glaciation.  
862 *Science* 334, 1261.
- 863 Pagani, M., J. C. Zachos, K. H. Freeman, B. Tipple, and S. Bohaty (2005). Marked decline in  
864 atmospheric carbon dioxide concentrations during the Paleogene. *Science* 309, 600–603.
- 865 Pälike, H., M. W. Lyle, H. Nishi, I. Raffi, A. Ridgwell, K. Gamage, A. Klaus, G. Acton,  
866 L. Anderson, J. Backman, J. Baldauf, C. Beltran, S. M. Bohaty, P. Bown, W. Busch, J. E. T.  
867 Channell, C. O. J. Chun, M. Delaney, P. Dewangan, T. Dunkley Jones, K. M. Edgar,  
868 H. Evans, P. Fitch, G. L. Foster, N. Gussone, H. Hasegawa, E. C. Hathorne, H. Hayashi, J. O.  
869 Herrle, A. Holbourn, S. Hovan, K. Hyeong, K. Iijima, T. Ito, S.-I. Kamikuri, K. Kimoto,  
870 J. Kuroda, L. Leon-Rodriguez, A. Malinverno, T. C. Moore, Jr., B. H. Murphy, D. P. Murphy,  
871 H. Nakamura, K. Ogane, C. Ohneiser, C. Richter, R. Robinson, E. J. Rohling, O. Romero,  
872 K. Sawada, H. Scher, L. Schneider, A. Sluijs, H. Takata, J. Tian, A. Tsujimoto, B. S.  
873 Wade, T. Westerhold, R. Wilkens, T. Williams, P. A. Wilson, Y. Yamamoto, S. Yamamoto,  
874 T. Yamazaki, and R. E. Zeebe (2012). A Cenozoic record of the equatorial Pacific carbonate  
875 compensation depth. *Nature* 488, 609–614.
- 876 Pearson, P. N., G. L. Foster, and B. S. Wade (2009). Atmospheric carbon dioxide through the  
877 Eocene-Oligocene climate transition. *Nature* 461, 1110–1113.
- 878 Pearson, P. N. and M. R. Palmer (2000). Atmospheric carbon dioxide concentrations over the  
879 past 60 million years. *Nature* 406, 695–699.
- 880 Pytkowicz, R. M. and J. E. Hawley (1974). Bicarbonate and carbonate ion-pairs and a model of  
881 seawater at 25°C. *Limnology and Oceanography* 19(2), 223–234.
- 882 Rae, J. W. B. (2018). Boron Isotopes in Foraminifera: Systematics, Biomineralisation, and CO<sub>2</sub>  
883 Reconstruction. In Marschall H., Foster G. (Ed.), *Boron Isotopes*, pp. 107–143. Springer.
- 884 Ramette, R. W. (2004). Gravimetric Titrations: In Support of Weight Titration Techniques. *J.*  
885 *Chem. Educ.* 81, 1715.
- 886 Rausch, S., F. Böhm, W. Bach, A. Klügel, and A. Eisenhauer (2013). Calcium carbonate veins in  
887 ocean crust record a threefold increase of seawater Mg/Ca in the past 30 million years. *Earth*  
888 *Planet. Sci. Lett.* 362, 215–224.
- 889 Raven, J. and K. Crawford (2012). Environmental controls on coccolithophore calcification. *Mar.*  
890 *Ecol. Progr. Ser.* 470, 137–166.
- 891 Ridgwell, A. and D. Schmidt (2010). Past constraints on the vulnerability of marine calcifiers to  
892 massive carbon dioxide release. *Nature Geosci.* 3, 196–200, doi:10.1038/ngeo755.

- 893 Ries, J. B. (2004). Effect of ambient Mg/Ca ratio on Mg fractionation in calcareous marine  
894 invertebrates: A record of the oceanic Mg/Ca ratio over the Phanerozoic. *Geology* 32, 981.
- 895 Robinson, R. A. and R. H. Stokes (1959). *Electrolyte solutions, 2nd ed.* London, pp. 559:  
896 Butterworth's.
- 897 Rohling, E. J., A. Sluijs, H. Dijkstra, R. v. d. W. P. Köhler, A. von der Heydt, D. Beerling,  
898 A. Berger, P. Bijl, M. Crucifix, R. deConto, S. Drijfhout, A. Fedorov, G. Foster, A. Ganopolski,  
899 J. Hansen, B. Hönlisch, H. Hooghiemstra, M. Huber, P. Huybers, R. Knutti, D. Lea, L. Lourens,  
900 D. Lunt, V. Masson-Demotte, M. Medina-Elizalde, B. Otto-Bliesner, M. Pagani, H. Pälike,  
901 H. Renssen, D. Royer, M. Siddall, P. Valdes, J. Zachos, and R. Zeebe (2012). Making sense of  
902 palaeoclimate sensitivity. *Nature* 497, 683–691, doi:10.1038/nature11574.
- 903 Rushdi, A. I. and A. C. Chen-Tung (1995). Variation of the apparent dissociation constants of  
904 carbonic acid with magnesium and calcium concentrations in seawater. *Terr., Atmos. Ocean.  
905 Sci.* 6(2), 347–361.
- 906 Rushdi, A. I., A. C. Chen-Tung, and E. Suess (1998). The solubility of calcite in seawater  
907 solution of different magnesium concentrations at 25°C and 1 atm total pressure: A laboratory  
908 re-examination. *La mer* 36, 9–22.
- 909 Seki, O., G. L. Foster, D. N. Schmidt, A. Mackensen, K. Kawamura, and R. D. Pancost (2010).  
910 Alkenone and boron-based Pliocene  $p\text{CO}_2$  records. *Earth Planet. Sci. Lett.* 292, 201–211.
- 911 Shi, W., A. T. Kan, N. Zhang, and M. Tomson (2013). Dissolution of calcite at up to 250°C and  
912 1450 bar and the presence of mixed salts. *Industr. Engineer. Chem. Res.* 52(6), 2439–2448.
- 913 Sosdian, S. M., R. Greenop, M. P. Hain, G. L. Foster, P. N. Pearson, and C. H. Lear (2018).  
914 Constraining the evolution of Neogene ocean carbonate chemistry using the boron isotope pH  
915 proxy. *Earth Planet. Sci. Lett.* 498, 362–376.
- 916 Stanley, S. M. and L. A. Hardie (1998). Secular oscillations in the carbonate mineralogy of  
917 reef-building and sediment-producing organisms driven by tectonically forced shifts in seawater  
918 chemistry. *Palaeogeogr., Palaeoclimatol., Palaeoecol.* 144, 3–19.
- 919 Stefánsson, A., P. Bénézech, and J. Schott (2013). Carbonic acid ionization and the  
920 stability of sodium bicarbonate and carbonate ion pairs to 200°C - A potentiometric and  
921 spectrophotometric study. *Geochim. Cosmochim. Acta* 120, 600–611.
- 922 Stefánsson, A., P. Bénézech, and J. Schott (2014). Potentiometric and spectrophotometric study  
923 of the stability of magnesium carbonate and bicarbonate ion pairs to 150°C and aqueous  
924 inorganic carbon speciation and magnesite solubility. *Geochim. Cosmochim. Acta* 138, 21–31.
- 925 Stefánsson, A., K. H. Lemke, P. Bénézech, and J. Schott (2017). Magnesium bicarbonate and  
926 carbonate interactions in aqueous solutions: An infrared spectroscopic and quantum chemical  
927 study. *Geochim. Cosmochim. Acta* 198, 271–284.
- 928 Sundquist, E. T. (1986). Geologic Analogs: Their value and limitations in carbon dioxide  
929 research. In J. R. Trabalka and D. E. Reichle (Ed.), *The Changing Carbon cycle: A Global  
930 Analysis*, pp. 371–402. Springer-Verlag, New York.
- 931 Sundquist, E. T. (1999). Seawater pH and atmospheric carbon dioxide. *Science* 286(5447), 2043a.
- 932 Super, J. R., E. Thomas, M. Pagani, M. Huber, C. O'Brien, and P. M. Hull (2018). North Atlantic  
933 temperature and  $p\text{CO}_2$  coupling in the early-middle Miocene. *Geology* 46, 519–522.
- 934 Timofeeff, M. N., T. K. Lowenstein, M. A. M. da Silva, and N. B. Harris (2006). Secular variation  
935 in the major-ion chemistry of seawater: Evidence from fluid inclusions in Cretaceous halites.  
936 *Geochim. Cosmochim. Acta* 70, 1977–1994.

- 937 Tyrrell, T. and R. E. Zeebe (2004). History of carbonate ion concentration over the last 100  
938 million years. *Geochim. Cosmochim. Acta* 68(17), 3521–3530.
- 939 Waters, J., F. J. Millero, and R. J. Woosley (2014). Corrigendum to "The free proton concentration  
940 scale for seawater pH", [MARCHE: 149 (2013) 8–22]. *Mar. Chem.* 165, 66–67.
- 941 Waters, J. F. and F. J. Millero (2013). The free proton concentration scale for seawater pH. *Mar.*  
942 *Chem.* 149, 8–22.
- 943 Wolf, M., O. Breitkopf, and R. Puk (1989). Solubility of calcite in different electrolytes at  
944 temperatures between 10° and 60°C and at CO<sub>2</sub> partial pressures of about 1 kPa. *Chem.*  
945 *Geol.* 76, 291–301.
- 946 Zeebe, R. E. (2012a). History of seawater carbonate chemistry, atmospheric CO<sub>2</sub>, and ocean  
947 acidification. *Annu. Rev. Earth Planet. Sci* 40, 141–165.
- 948 Zeebe, R. E. (2012b). LOSCAR: Long-term Ocean-atmosphere-Sediment Carbon cycle Reservoir  
949 Model v2.0.4. *Geosci. Model Dev.* 5, 149–166.
- 950 Zeebe, R. E. and T. Tyrrell (2018). Comment on "The effects of secular calcium and magnesium  
951 concentration changes on the thermodynamics of seawater acid/base chemistry: Implications  
952 for Eocene and Cretaceous ocean carbon chemistry and buffering". *Global Biogeochem. Cycles* 32,  
953 10.1002/2017GB005786.
- 954 Zeebe, R. E. and D. A. Wolf-Gladrow (2001). *CO<sub>2</sub> in Seawater: Equilibrium, Kinetics, Isotopes.*  
955 Amsterdam, pp. 346: Elsevier Oceanography Series.
- 956 Zeebe, R. E., J. C. Zachos, and G. R. Dickens (2009). Carbon dioxide forcing alone insufficient  
957 to explain Palaeocene-Eocene Thermal Maximum warming. *Nature Geosci.* 2, 576–580,  
958 doi:10.1038/ngeo578.
- 959 Zhang, Y. G., M. Pagani, Z. Liu, S. M. Bohaty, and R. DeConto (2013). A 40-million-year history  
960 of atmospheric CO<sub>2</sub>. *Phil. Trans. Royal Soc. London A* 371, 20130096–20130096.
- 961 Zhou, X., W. Si, J. Erez, and Y. Rosenthal (2018). Foraminiferal Na/Ca suggests decreased  
962 seawater Ca concentration and reduced hydrothermal activity since Mid-Miocene. In  
963 *Goldschmidt Abstracts 2018.*